University of Kent

Kent Academic Repository

Dui, Hongyan, Guo, Weina, Xia, Wanyun and Wu, Shaomin (2025) *Digital twin-based resilience analysis and emergency maintenance with generative AI of smart urban metro systems*. Reliability Engineering and System Safety, 265 (Part A). ISSN 0951-8320.

Downloaded from
https://kar.kent.ac.uk/111027/ The University of Kent's Academic Repository KAR

The version of record is available from
https://doi.org/10.1016/j.ress.2025.111537

This document version
Author's Accepted Manuscript

DOI for this version

Licence for this version
CC BY (Attribution)

Additional information
For the purpose of open access, the author(s) has applied a Creative Commons Attribution (CC BY) licence to any Author Accepted Manuscript version arising.

Versions of research works

Versions of Record
If this version is the version of record, it is the same as the published version available on the publisher's web site. Cite as the published version.

Author Accepted Manuscripts
If this document is identified as the Author Accepted Manuscript it is the version after peer review but before type setting, copy editing or publisher branding. Cite as Surname, Initial. (Year) 'Title of article'. To be published in ***Title of Journal*** , Volume and issue numbers [peer-reviewed accepted version]. Available at: DOI or URL (Accessed: date).

Enquiries
If you have questions about this document contact ResearchSupport@kent.ac.uk. Please include the URL of the record in KAR. If you believe that your, or a third party's rights have been compromised through this document please see our Take Down policy (available from https://www.kent.ac.uk/guides/kar-the-kent-academic-repository#policies).

Digital twin-based resilience analysis and emergency maintenance with generative AI of smart urban metro systems

Hongyan Dui[a], Weina Guo[a], Wanyun Xia[a*],Shaomin Wu[b]

[a]School of Management, Zhengzhou University, Zhengzhou 450001, China

[b]Kent Business School, University of Kent, Canterbury, Kent CT2 7FS, UK

Abstract: With the rapid expansion and growing complexity of urban metro systems, operational disturbances increasingly threaten system stability and service continuity. However, existing recovery strategies remain insufficient in terms of emergency response efficiency and intelligent decision-making. To address these challenges, this study proposes a digital twin metro system architecture with generative AI, enabling real-time system status monitoring and optimized emergency maintenance decision-making. A cascading failure model is developed to reveal the regulatory role of nonlinear capacity parameters in failure propagation and to demonstrate its practical applicability. Furthermore, the study investigates performance and cost variations across failure and recovery phases, and introduces a cost importance-based recovery strategy that enhances system resilience by optimizing the station recovery sequence. Finally, using the Beijing metro as a case study, the impact of different recovery strategies is evaluated under both single-line section and multi-line section attack scenarios. The results indicate that the cost importance-based strategy (CIBRS) outperforms traditional approaches (BBRS, DBRS, ECBRS, RGBRS). In the single-line section attack, it achieves a resilience value of 0.747, with improvements of 74.94%, 35.34%, 95.55%, and 1.91%, respectively. Under the multi-line section attack, the resilience value reaches 0.777, with corresponding improvements of 79.45%, 46.33%, 85.44%, and 5.00%. The result confirms the superior adaptability and robustness of the proposed method in complex scenarios. This study offers valuable insights for intelligent metro system management and emergency maintenance.

Keywords: digital twin; resilience; emergency maintenance; generative AI; urban metro system

1. Introduction

With the rapid development of urbanization, the urban population has increased significantly. Limited land resources, traffic congestion, and environmental issues caused by the rapid population growth make the

* Corresponding author. xiawanyun1989@126.com Tel: (86) 371- 67781582, Fax: (86) 371- 67781582.

development of urban underground space one of the key prerequisites for sustainable urban development [1]. Metros has been widely applied to enhance the level of urban resilience, such as enhancing urban compactness [2], strengthening spatial accessibility [3], and creating low carbon cities [4]. However, the metro is susceptible to attacks from natural disasters and man-made disasters, such as the Zhengzhou metro flooding in China in 2021, the Yekaterinburg metro tunnel fire in Russia in 2022, and the Boston train suspension in the USA due to an underground pipe rupture in 2023, all of which caused significant economic losses or casualties. The cascading failure of the metro system in response to disasters severely restricts the development of its safety and reliability. Current metro maintenance strategies still rely primarily on periodic plans or manual experience, lacking the ability for precise perception of system status and dynamic adjustment. This frequently leads to excessive or insufficient maintenance, thereby affecting system reliability and increasing operational and maintenance costs. In this context, the digital twin (DT) connects physical systems with virtual models, enabling real-time monitoring, fault prediction, and maintenance optimization [5]. It offers a novel approach to achieving more accurate, intelligent, and visualized metro system operation and maintenance.

As a critical bridge between the physical and virtual worlds, DT plays an essential role in system modeling and simulation [6]. It has been applied to real-time monitoring of complex systems, the implementation of autonomous control systems, and assistance during accidents and emergencies [7–10]. However, with the continuous development of cities, systems are becoming increasingly complex, posing numerous challenges to existing DT systems, such as data collection interruptions, poor modeling of special scenarios, and inefficient data processing. These limitations often result in incomplete and missing data, leading to decreased accuracy or even failure of predictive models [11]. Some studies have addressed the challenges of incomplete or limited data in system maintenance by introducing data-enhanced fault prediction models and uncertainty-based degradation modeling methods. For example, Shao et al. introduced an innovative method for remaining useful life prediction using small sample data, where the interaction between data and the model is leveraged to assess equipment reliability and remaining useful life [12]. Cai et al. established the structure and parameter models of dynamic Bayesian networks for single-factor degradation processes based on theoretical or empirical physical models, effectively addressing the issue of limited data availability [13]. A remaining useful life re-prediction method for complex systems based on the Wiener process improved prediction accuracy by effectively integrating historical data with online monitoring data [14]. These studies provide effective solutions for predictive modeling and performance evaluation under data-limited conditions. However, they remain insufficient in terms of system-level modeling, response mechanism simulation under complex scenarios, and intelligent optimization of maintenance

strategies. To overcome these limitations, generative AI leverages its powerful data processing and scenario generation capabilities. When integrated with DT, it enables efficient modeling, accurate prediction, and intelligent decision-making for complex systems under conditions of limited data or high uncertainty. Leveraging the powerful data processing capabilities of generative AI, Huang et al. proposed a generative AI-driven DT network architecture to enhance network management performance. In this architecture, various generative AI models can be utilized to support status emulation, feature extraction, and intelligent decision-making within the DT [15]. Mata et al. present a novel integration of human expertise and generative AI within a DT design framework [16] The integrated application of DT and generative AI in metro systems not only enhances the system's capabilities in perceiving, responding to, and recovering from unexpected events, but also offers great potential for enabling more intelligent, scalable, and automated urban development and management.

Achieving the reliability and sustainable operation of infrastructure systems often requires substantial cost investment. Many studies have explored the relationship between different system performances and costs. Chen et al. [17] developed a maintenance cost rate function, which connected the constructed remaining useful life distribution with maintenance-related costs. Li et al. [18] quantified the effects of different uncertainties on offshore wind farms through maintenance costs and production losses. Dui et al. [19] developed a new multi-status system performance efficiency and cost analysis model with continuous damage and recovery in multiple shock events. Han et al. [20] developed a three-dimensional performance-time-cost space to interpret composite performance and recovery costs. In the metro system, the service capacity of each station and line in meeting passenger travel demands is evaluated by measuring the flow at each station and line, thereby quantifying the performance and functionality of the metro system. Xu et al. [21] developed a metro station resilience analysis methodology by integrating infrastructure characteristics and passenger flow dynamics. Lu et al. [22] studied cascading failures integrating network topology and passenger flow. Dui et al. [23] considered the cascading failures in unmanned vehicle power distribution networks under different conditions. They integrated failure times into maintenance strategies to real-time path changes to increase the reliability of accomplishing distribution tasks and improve resilience after congestion. Cai et al. [24] noted that Bayesian networks offer significant advantages in modeling uncertainty and handling complex dependencies, providing valuable support for system performance prediction and maintenance decision-making. Chen et al. [25] proposed a passenger-oriented resilience evaluation model for urban rail transit networks, in which the performance indicator captures the impact of travel time distribution on overall network performance. Metro revenue is closely related to passenger flow, and fluctuations in passenger flow at failed stations will cause metro cost losses [26]. Therefore, this study uses revenue variation

caused by passenger flow fluctuations to reflect changes in system performance, evaluating metro operations under disturbances. In complex networks, failures often propagate in a cascading manner, resulting in overall system performance degradation. A thorough analysis of the failure evolution process facilitates the identification of propagation paths and critical nodes, thereby providing a theoretical foundation for the formulation of effective recovery strategies and the improvement of maintenance efficiency. Zhang et al. [27] proposed a cascading reliability model for modeling, measuring, and controlling multimodal public transportation networks with cascading failures. Lu et al. [28] proposed an enhanced coupled map lattice model to solve the evolution process of cascading failures in rail transit networks. The model combines quantitative fault expansion modes, station risk resistance capabilities, and attack indices to quantify the important influencing factors of cascading failures. Zhang et al. [29] analysed the passenger dynamics and station status of urban rail transit networks under three types of malicious attacks used to simulate external interference. Analyzing the cascading failure process of complex networks helps to determine the failure scale and grasp the entire system's stable operation based on the characteristics of cascading failures.

Based on the identification of critical failure nodes, further quantifying the system's ability to maintain functionality and recover under disturbances has become a central focus in resilience research. Topology-based methods evaluate infrastructure performance and vulnerability by analyzing variations in structural characteristics, while flow-based methods assess performance in terms of functionality loss [30], resilience evaluation [31,32], and resilience optimization [33–35]. Xing et al. [36] established a metro line topology model based on the real connection relationship of metro stations. System remaining performance depends on the distance between section center and line center, passenger flow loss, and the number of stations in the section. Yu et al. [37] proposed a Functional Connectivity Analysis (FCA) method that incorporates flow-related characteristics into topological connectivity metrics, enabling functionality evaluation comparable to flow-based methods while maintaining computational efficiency similar to connectivity analysis. Wang et al. [38] proposed a dynamic resilience evaluation index that integrates passenger demand and infrastructure supply to evaluate metro system performance. Ma et al. [39] constructed a life-cycle resilience evaluation model for urban rail transit, oriented towards passenger travel service. The results indicate that the importance of stations depends not only on topology but also on passenger flow. Cai et al. [40] developed a resilience evaluation methodology that combines Markov models and dynamic Bayesian networks to assess system resilience under varying external disasters. He et al. [41] conducted a comprehensive examination of underground transport networks' flood vulnerability and recoverability and performed a specific analysis to assess their flood resilience. Within the framework of complex network analysis,

Yu et al. [42] established an accessibility-resilience-serviceability three-dimensional framework to quantify the service performance of an urban metro network within the complex network analysis. Cai et al. [43] proposed a new availability-based engineering resilience metric from the perspective of reliability engineering. In summary, existing resilience evaluation studies have encompassed various aspects such as topological structure, flow characteristics, and service performance. These studies provide theoretical support for performance analysis and strategy optimization of metro systems under disruptions.

Emergency maintenance plays a critical role in ensuring the stability of system performance and enabling rapid recovery. In complex systems, cascading failures can lead to multiple parts failing [44]. Different stations have varying impacts on system performance. The efficiency of emergency maintenance largely depends on the rationality and optimization of the recovery sequence. An optimized recovery sequence can not only reduce resource consumption but also enhance the timeliness of emergency responses and the overall resilience of the system [45,46]. In recent years, there has been extensive research on the development and optimization of system maintenance strategies [47–50] Song et al. proposed a resilience-based sequential recovery strategy that considers varying node recovery time and resource limitations [51]. Hu et al. explored a seismic resilience evaluation method considering the effect of infrastructure interdependency and proposed a two-stage functional recovery optimization model [52]. Wang et al. present a resilience analysis framework based on importance, evaluating affected components at various disturbance stages to optimize system resilience [53]. Zhang et al. [54] proposed two importance measures to evaluate component priority and guide the selection of efficient maintenance sequences. Therefore, a well-designed recovery sequence is highly significant for improving emergency maintenance efficiency and enhancing system resilience.

The complexity of urban metro infrastructure and the variability of passenger flows necessitate real-time monitoring and adaptive maintenance strategies to ensure resilient operations. However, existing research pays insufficient attention to the costs caused by passenger flow variations and the prioritization of station recovery, and lacks precision in system status perception and dynamic adjustments, resulting in low emergency maintenance efficiency. Therefore, this paper proposes a resilience evaluation method and emergency maintenance strategy based on DT and generative AI. The main contributions are summarized as follows.

(1) A DT metro system framework integrated with generative AI is developed in the paper, and structural support for real-time monitoring and maintenance optimization is provided.

(2) A resilience evaluation model incorporating cascading failure and two-stage costs is proposed. The cascading failure model reveals the regulatory role of nonlinear capacity parameters in the process of failure

propagation, while the two-stage cost quantifies the impact of passenger flow variations during the damage-recovery process.

(3) A cost importance-based recovery strategy is introduced to optimize system recovery efficiency under limited resources. The strategy aims to significantly enhance system resilience and emergency maintenance efficiency by accurately identifying the recovery priorities of stations in the metro network.

The remaining of the paper is structured as follows. **Section 2** proposes a digital twin urban metro system architecture with generative AI, and simulates cascading failures. **Section 3** analyses the resilience evaluation of urban metro system considering passenger flow changes during the failure and recovery process. **Section 4** focuses on emergency maintenance of urban metro system and proposes a novel recovery strategy for resilience enhancement. **Section 5** presents the case study. **Section 6** gives conclusions and several future research directions.

2. Proposed Digital Twin Architecture with Generative AI of Smart Urban Metro Systems

To address resilience evaluation and emergency maintenance in the urban metro system, this paper proposes an intelligent metro system architecture based on DT and generative AI. Specifically, the proposed DT metro system constructs a highly accurate virtual replica of the metro system through real-time data acquisition, transmission, and analysis. This enables real-time monitoring of operational status, fault detection, performance prediction, and maintenance optimization. The system operates through the coordinated functioning of perception, data, model, and application layers, with innovative integration of generative AI technologies to enhance management efficiency and recovery capabilities of metro systems. The specific architectural is shown in **Fig. 1.**

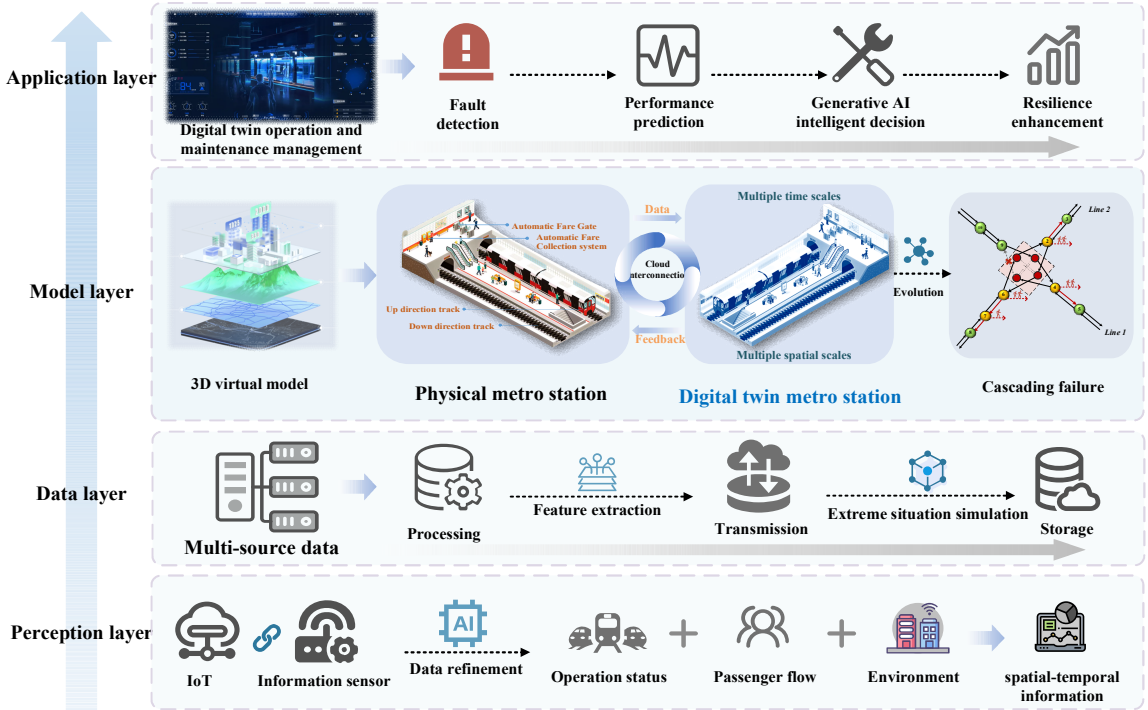


Fig. 1. The architecture of digital twin metro system

In the perception layer, IoT devices and information sensors monitor the operational status of metro infrastructure (e.g., tracks and trains) in real time, passenger flow, environment and spatial-temporal information for the DT system. The data layer processes multi-source data through feature extraction, transmission, and storage, leveraging generative AI to simulate extreme situations and deliver high-quality data to the model layer. Centered on the DT metro station, the model layer integrates 3D virtual models to perform cross-temporal and spatial simulation analyses. This enables prediction of evolving trends such as passenger flow anomalies and cascading failures, achieving precise mapping of the physical metro station. The application layer employs generative AI for fault detection, performance prediction, and intelligent decision-making. It evaluates the impact of maintenance strategies on system recovery, visualizes system status through an interactive interface, and enhances operational resilience. The entire architecture revolves around the DT, forming an iterative cycle for optimizing physical perception, virtual simulation, and decision-making. This integrated framework encompasses status monitoring, proactive control, and performance optimization, ensuring the metro system's efficient and reliable operation.

As the primary interface through which the DT system perceives the physical world, the perception layer serves as the foundational component for data acquisition, model development, and application deployment. It also forms the core basis for the design of the data layer, model layer, and application layer. Therefore, this paper focuses on the modeling and analysis of the perception layer, aiming to lay the foundation for achieving precise mapping and optimized control of physical entities. The metro system consists of multiple stations and sections between stations, and its spatial relationship is relatively complex. In this section, to make the spatial position and connection of the metro network more intuitive, the shape of the edges is no longer considered, and a spatial model is used for research regarding metro stations as nodes and line sections as edges. Since the direction of the tracks inside the metro system is strictly regulated, this paper constructs a bidirectional metro network $G = (S, E)$ composed of n nodes, among which S and E are sets of nodes, and directed edges, $S = \{S_i\}, i = 1,2,\cdots,n,\ E = \{e_{ij}\}, j = 1,2,\cdots,n$, where e_{ij} indicate the section from S_i to S_j. To accurately represent the train operation directions within stations, this paper constructs a bidirectional metro network to describe the real dispersion of passenger flow. A simplified diagram of the metro network is shown in **Fig. 2**.

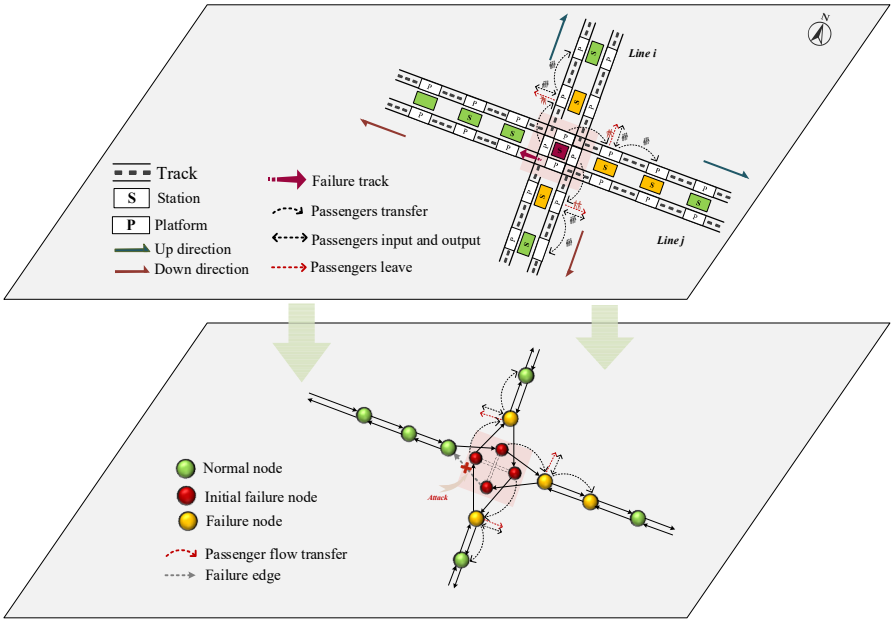


Fig. 2. Simplified diagram of metro network nodes and edges

For a metro network with n nodes, the adjacency matrix $\boldsymbol{A}$ is a n dimension matrix, where $a_{i,j}$ indicates the directed connection relationship between S_i and S_j expressed as shown in **Eq. (1)**,

$$\boldsymbol{A} = \begin{bmatrix} a_{1,1} & \cdots & a_{1,n} \\ \cdots & a_{i,j} & \cdots \\ a_{n,1} & \cdots & a_{n,n} \end{bmatrix}, \tag{1}$$

$$a_{i,j} = \begin{cases} 1 & i \text{ and } j \text{ are connected directly} \\ 0 & \text{otherwise} \end{cases}.$$

Denote the degree of S_i by D_i, $D_i = \sum_{j=1}^{n} a_{i,j}$ and indicate the betweenness of the network by B_i. $B_i = \sum_{l \neq k} \frac{n_{l,k}(i)}{n_{l,k}}$, where $n_{l,k}(i)$ is the number of the shortest paths from S_l to S_k passing through S_i, and $n_{l,k}$ is the total number of the shortest paths from S_l to S_k.

When one or more sections of the metro system fail, passengers from the starting station of the section cannot board and leave, so the starting station fails due to the retention of many passengers. To arrive at the destination in time, some passengers leave the metro system and choose other means of transportation, but most passengers still stay in the metro system. They choose to transfer to the neighboring station. The passenger option at the failed station is shown in **Fig. 3**. However, the capacity of metro stations is limited by physical space, facility level, and other factors. When many passengers need to be transferred due to a failed station, some neighboring stations will also become congested due to too many passengers, causing passengers to transfer again.

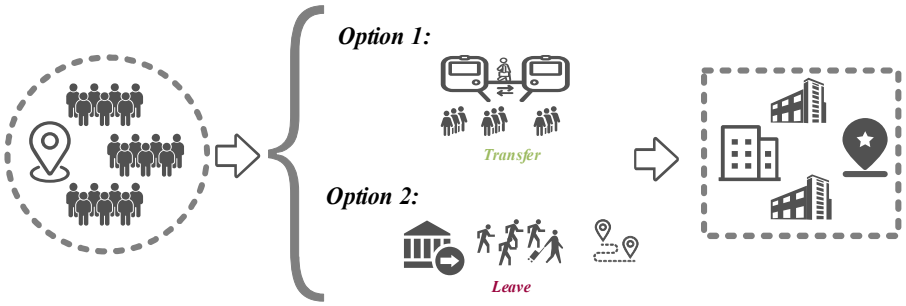


Fig. 3. Passenger transfer process

For the convenience of research, this section is based on the nonlinear load-capacity model to construct a cascading failure model for the metro network. Nodes in the network are divided into normal and failed status, where nodes that accept transferred passenger flow and become overloaded (i.e., load more than capacity) are considered failed nodes. Failed nodes will not automatically recover to the normal status during the cascading failure period. To truly reflect the impact of passenger flow transfer on the status of stations, the cross-sectional average passenger flow is taken as the initial load, the load of the node $F_i = F_i^{Nor}$ in the normal status, of the node when it is normally operating. The capacity of the node is a nonlinear relationship with the initial load [55], and can be represented as

$$Q_i = F_i^{Nor} + \beta \cdot (F_i^{No})^{\alpha}, \tag{2}$$

where α and β indicate the tolerance parameter of the metro network.

Before being attacked, all nodes in the network are considered normal. At a certain moment t, a failure occurs in the section e_{ij} from S_i to S_j, and all passenger flow F_{ij} of the section is stranded at the starting S_i of the section. Passengers within the capacity range will choose to wait in place, while passengers exceeding the capacity Q_i will leave the system in proportion k, and the remaining passengers exceeding the capacity will be transferred to neighboring nodes. During the load distribution process, the passenger flow leaving from the S_i is

$$\Delta F_i^{Leave}(t) = k \cdot \left(F_i^{Nor} + F_{ij}(t) - Q_i\right). \tag{3}$$

The sum of passenger flows transferred from the S_i to its neighboring stations is

$$\Delta F_i^{Transfer}(t) = (1-k) \cdot \left(F_i^{Nor} + F_{ij}(t) - Q_i\right), \tag{4}$$

where the passenger flow transferred to the neighboring S_d is

$$\Delta F_{i\to d}^{Transfer}(t) = Z_d \cdot \Delta F_i^{Transfer}(t), \tag{5}$$

$$Z_d = \frac{Q_d}{\sum_{d\in\tau^i} Q_d}, \tag{6}$$

where Z_d indicates the proportion of the load of the failed node borne by the neighboring node S_d; τ^i indicates the set of neighboring nodes of the failed node S_i. Therefore, the passenger flow transferred from the failed node S_i to

its neighboring node S_d can be expressed as

$$\Delta F_{i\to d}^{Transfer}(t) = (1-k)\cdot\frac{Q_d}{\sum_{d\in\tau^i} Q_d}\cdot\left(F_i^{Nor} + F_{ij}(t) - Q_i\right). \tag{7}$$

After the transfer time $\Delta t^{Transfer}$, the final flow of the S_i is the node capacity, i.e.,

$$F_i^{Final}\left(t + \Delta t_1^{Transfer}\right) = Q_i. \tag{8}$$

The passenger flow transferred from S_i arrives at S_w at time $t + \Delta t^{Transfer}$, at this time, the new load F_d^{Now} of S_d is

$$F_d^{Now}\left(t + \Delta t_1^{Transfer}\right) = F_d^{Nor} + \Delta F_{i\to d}^{Transfer}(t). \tag{9}$$

It is necessary to assess the relationship between the new load $F_d^{Now}\left(t + \Delta t_1^{Transfer}\right)$ of the node and its capacity Q_d. If $F_d^{Now}\left(t + \Delta t_1^{Transfer}\right) > Q_d$, the S_w is a failed node. The load exceeding the node capacity still needs to leave the system in proportion k, and the remaining load exceeding the capacity is transferred to its neighboring stations. However, due to the directionality of metro operation, the load of the failed node will only be allocated to downstream nodes. It will not be transferred to upstream failed nodes, so the load will no longer be allocated to the S_i. Assuming $F_d^{Now}\left(t + \Delta t_1^{Transfer}\right) > Q_d$ still exists, taking a neighboring node S_h of S_d as an example, the specific load distribution situation is

$$\Delta F_d^{Leave}\left(t + \Delta t_1^{Transfer}\right) = k\cdot\left(F_d^{Now}\left(t + \Delta t_1^{Transfer}\right) - Q_d\right), \tag{10}$$

$$\Delta F_d^{Transfer}\left(t + \Delta t_1^{Transfer}\right) = (1-k)\cdot Z_h\cdot\left(F_d^{Now}\left(t + \Delta t_1^{Transfer}\right) - Q_d\right), \tag{11}$$

$$Z_h = \frac{Q_h}{\sum_{h\in\tau^w, h\neq i} Q_h}, \tag{12}$$

and

$$\Delta F_{d\to h}^{Transfer}\left(t + \Delta t_1^{Transfer}\right) = (1-k)\cdot\frac{Q_h}{\sum_{h\in\tau^d, h\neq i} Q_h}\cdot\left(F_d^{Now}\left(t + \Delta t_1^{Transfer}\right) - Q_d\right). \tag{13}$$

After time $\Delta t_2^{Transfer}$, the final capacity at S_d is

$$F_d^{Final}\left(t + \Delta t_2^{Transfer}\right) = Q_d. \tag{14}$$

At this time, the new load F_h^{Now} of the S_h is

$$F_h^{Now}\left(t + \Delta t_2^{Transfer}\right) = F_h^{Nor} + \Delta F_{d\to h}^{Transfer}\left(t + \Delta t_1^{Transfer}\right). \tag{15}$$

After each round of the load distribution, it is necessary to assess the relationship between the load and its capacity of all nodes in the network. Suppose nodes have new loads more than their capacity. In that case, the above rules will be followed for the load distribution in a hierarchical manner until the load of all nodes in the network does not exceed the capacity, and the cascading failure ends.

The following takes the attack on S_1 as an example to illustrate a typical process, as shown in **Fig. 4**. S_1 is a transfer station between Lines 1 and 2. For the convenience of analysis, based on the operation direction of the metro, S_1 is divided into four sub-nodes S_{1N}, S_{1S}, S_{1E}, S_{1W}.

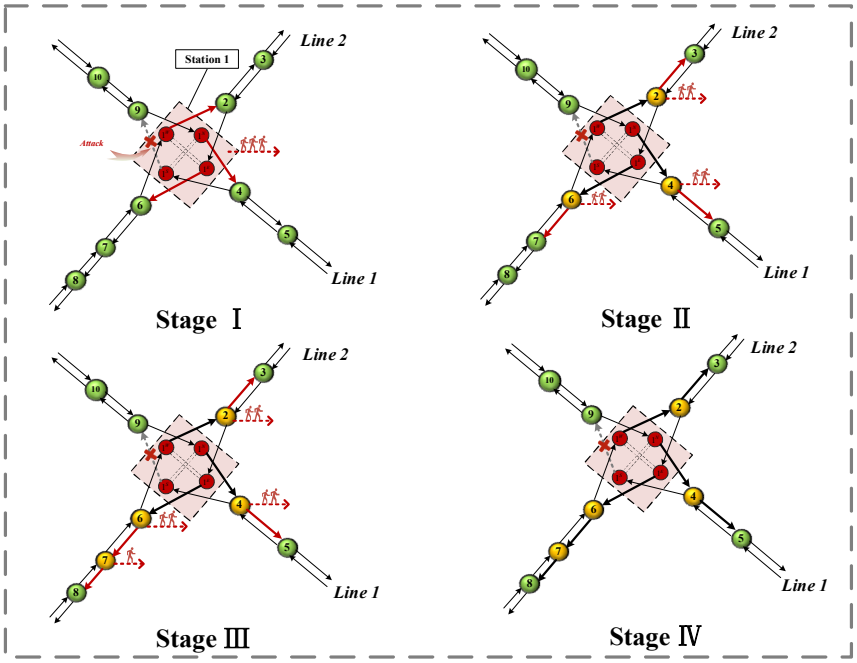


Fig. 4. The cascading failure process of the metro network

Stage Ⅰ : e_{1^S9} is disturbed, and many loads are stranded at S_1, causing S_1 to fail. The load exceeding the capacity of S_1 leaves the system based on **Eq. (4)**, and the remaining load is allocated to its neighboring nodes based on **Eq. (3)**, including S_2, S_4 and S_6. The final load of S_1 is its capacity.

Stage Ⅱ : Compare the new load and its capacity of the three neighboring nodes. All three stations fail. The load exceeding the node capacity still leaves the system based on **Eq. (4)**, and the remaining load of S_2 is transferred to S_3, the remaining load of S_4 is transferred to S_5, and the remaining load of S_6 is transferred to S_7.

Stage Ⅲ: Compare the new load and its capacity of S_3, S_5 and S_7. S_3 and S_5 are still normal because their new loads do not exceed the capacity. S_7 fails due to overload and allocates the load based on the above rules.

Stage Ⅳ: S_8 accepts the load from S_7 based on **Eq. (3)** and does not experience overload. At this point, no new failed nodes appear in the network, and the cascading failure ends.

It can be seen from **Fig. 4** that due to the attack of e_{1^S9}, S_1 fails first, then S_2, S_4 and S_6 fail, and finally, S_7 fails. We assume that the cascading failure process occurs hierarchically, and the load transfer at the same level is considered to occur and arrive at neighboring nodes.

3. Resilience Evaluation of Urban Metro System considering Passenger Flow Changes

When a metro station fails, the number of passengers decreases, and it even increases after returning to normal. The loss of passenger flow is inevitable in the entire process of damage and recovery of the metro system, which is usually directly reflected in the decline of operating income. Therefore, we use metro revenue P_i to represent the changes in system performance.

$$P_i(t) = F_i(t) \cdot p, \tag{16}$$

$$P(t) = \sum_{i=1}^{n} P_i(t), \tag{17}$$

where $P_i(t)$ indicates the revenue of S_i, p represents the average fare for a metro ride, $P(t)$ represents the revenue of the entire metro system at time t. At different times, the passenger flow is different, and the revenue is different. The higher the revenue, the better the network performance.

When a metro network is disturbed by external factors, some passengers choose to leave the system. The metro revenue decreases, and the network performance then gradually declines. After maintenance and recovery, the passengers who left the failed stations gradually return to the system, and the metro revenue increases, and the network performance gradually returns to its initial status. The resilience curve is often used to represent the above process, conveying the quantitative and qualitative aspects of system behavior and resilience to critical infrastructure stakeholders [56]. Passengers need time to transfer from the failed station to the neighboring station, during which the system performance remains at the same level. Therefore, this paper considers the performance of the metro network to change stepwise during the failure process. The performance of the network recovery stage also changes in steps because it takes a certain recovery time for the failed station to recover from the failure status to the normal status, and in the case of limited resources, only one station can be recovered at a time, and the recovery stages between stations is independent. The decline and enhancement of metro network performance both occur within $[0, t_s]$. To evaluate the performance changes of the system under specific attacks, the system performance is usually divided into failure, evolution, and recovery stages, and the damage-recovery process is evaluated by the concept of resilience. For the convenience of explanation, this paper divides the network performance change into three stages: normal, failure evolution, and recovery (**Fig. 5**).

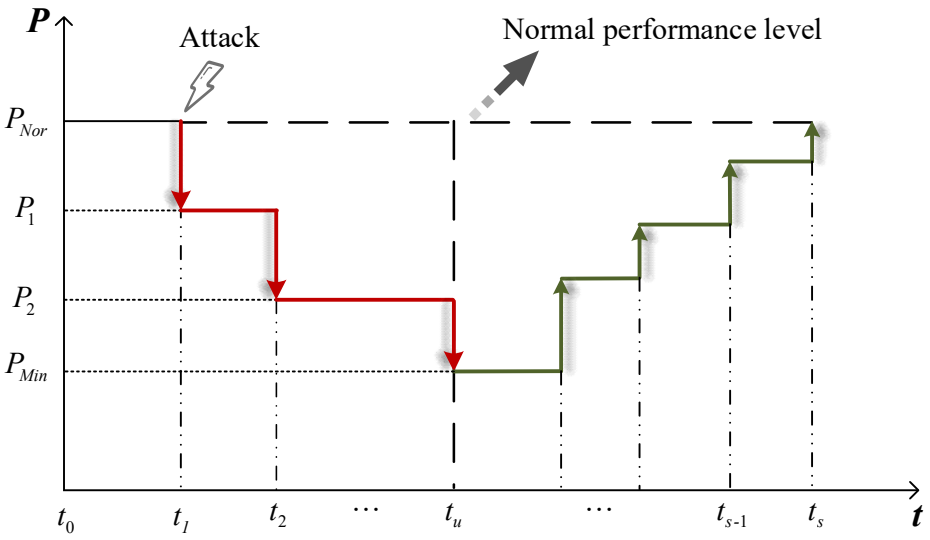


Fig.5. Changes of metro system performance after attack

(1) **Normal stage**: $t \in [t_0, t_1], P = P_{Nor}$. The metro system has not been disturbed, the entire network is in the best operating status, and the metro revenue is normal.

(2) **Failure evolution stage**: $t \in (t_1, t_m]$. The metro system is disturbed at time t_1. At this time, some passengers in the failed stations leave the metro system, and some passengers are transferred to its neighboring stations after $\Delta t_1 = t_2 - t_1$. The cascading failure caused by overload continues to reduce the metro revenue, and the network performance gradually declines. At time $t = t_m$, the performance of the metro network decreases to the lowest level P_{Min}.

(3) **Recovery stage**: $t \in (t_m, t_s]$, the maintenance and recovery of the failed stations begin at time $t = t_m$, and passengers gradually return to the metro system, improving the system performance. At time $t = t_s$, the performance of the metro recovers to its initial status P_{Nor}, and then maintains a stable operation.

It can be seen that $P(t)$ is a piecewise function whose expression can be written as

$$P(t) = \begin{cases} P_{Nor} & t_0 \le t < t_1 \\ P_1 & t_1 \le t < t_2 \\ \vdots & \vdots \\ P_{Min} & t_m \le t < t_{m+1} \\ \vdots & \vdots \\ P_{s-1} & t_{s-1} \le t < t_s \\ P_{Nor} & t = t_s \end{cases}. \tag{18}$$

Some metro systems are densely populated with passengers. Once a disaster occurs, passenger safety is severely tested, and the metro system's potential revenue loss is also significant. During the damage-recovery process, the loss and return of passenger flow in the metro system require a certain amount of time. There is a revenue loss compared to the normal operation status during this time. This paper refers to revenue loss as the cost of the metro system. Specifically, based on the meaning of performance in different stages, the cost can be divided

into the direct cost during the failure stage and the indirect cost during the recovery stage (**Fig. 6**).

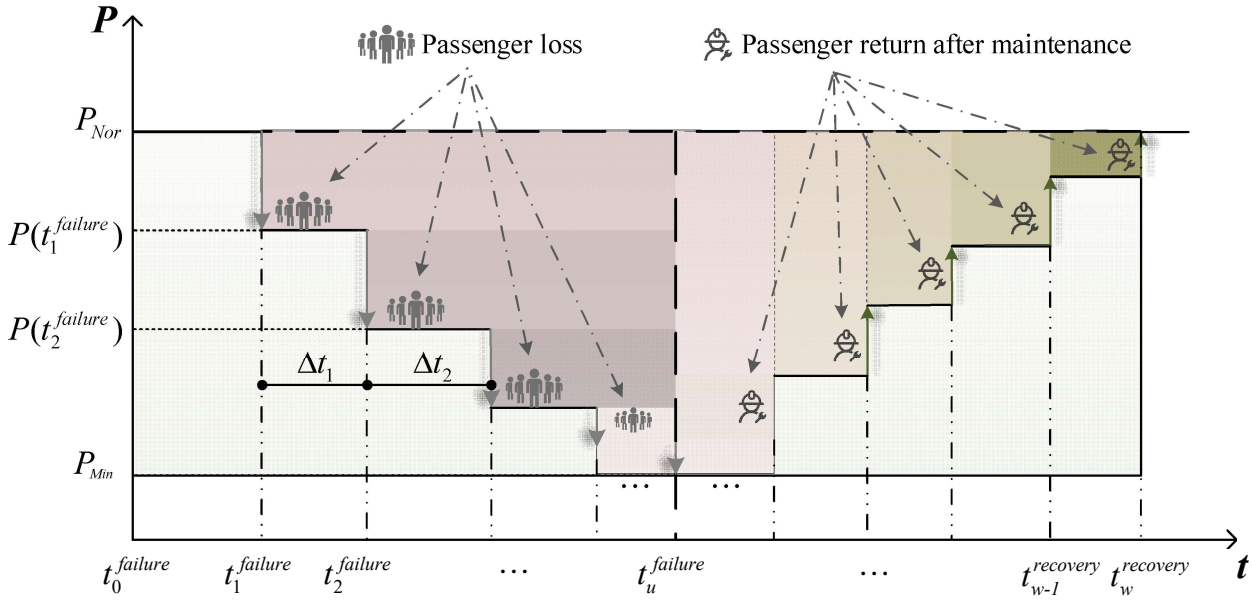


Fig. 6. Changes in metro network performance during the failure and recovery stages

During the failure evolution stage, the passenger flow at the failed stations decreases until the cascading failure ends. Based on past experience, the propagation time of the same level of failure is the same, so the decrease in metro performance at a certain moment during the failure stage indicates the sum of the revenue reduction of the new failed stations at that moment, i.e., the sum of the direct costs of the new failed stations at that moment. The cumulative value $S^D(t)$ of the direct cost at time t is

$$S^D(t)=\begin{cases}\sum_{\theta=1}^{u-1}\left[P\left(t_{\theta-1}^{failure}\right)-P\left(t_{\theta}^{failure}\right)\right]\left(t-t_{\theta}^{failure}\right), & t\in\left[t_1^{failure},t_u^{failure}\right)\\ \sum_{\theta=1}^{u-1}\left[P\left(t_{\theta-1}^{failure}\right)-P\left(t_{\theta}^{failure}\right)\right]\left(t_u^{failure}-t_{\theta}^{failure}\right), & t\in\left[t_u^{failure},t_w^{recovery}\right]\end{cases}, \tag{19}$$

where $\theta\in U,\ U=\{1,2,\cdots,u\}$, u indicates the total number of cascading failures, and at $t=t_u^{failure}$, the system performance reaches the lowest level, i.e., $P\left(t_u^{failure}\right)=P_{Min}$.

During the recovery stage, even though the passenger flow reduced at the failed stations will gradually recover, since only one station can be recovered at a time during the recovery period, the passenger flow at the stations that have not yet been recovered is still lost compared to the normal operation level. The difference between the actual and normal revenue during this stage is recorded as the indirect cost. The cumulative value $S^{ID}(t)$ of the indirect cost at time t is

$$S^{ID}(t)=\begin{cases}0, & t\in\left[t_1^{failure},t_u^{failure}\right)\\ \sum_{\partial=1}^{w}\left[P_{Nor}-P\left(t_{\partial-1}^{recovery}\right)\right]\left(t_{\partial}^{recovery}-t_{\partial-1}^{recovery}\right), & t\in\left[t_u^{failure},t_w^{recovery}\right]\end{cases}, \tag{20}$$

where $\partial \in W,\ W = \{1,2,\cdots,w\}$, w indicates the total number of failed stations. The metro system can return to its initial performance status after recovery, i.e., $P\left(t_w^{recovery}\right) = P\left(t_0^{failure}\right) = P_{Nor}$.

Throughout the damage-recovery process, the cost of the metro system $S^{Loss}(t)$ can be expressed as

$$S^{Loss}(t) = S^{D}(t) + S^{ID}(t). \tag{21}$$

Under the normal status, the total performance loss (i.e., cost) that the metro system can withstand is called the system performance margin S^{Margi} , i.e., the potential maximum cost when the system is facing attacks, $S^{Margin}(t)$ represented as

$$S^{Margi}\ (t) = [P_{Nor} - P(t)]\left(t - t_0^{failure}\right), t \in [t_0^{failure}, t_w^{recovery}]. \tag{22}$$

This paper defines resilience $R(t)$ as the ability of the metro system to absorb, adapt, and recover from the impacts of disasters, which is quantified as the ratio of the actual performance maintained to the potential maximum performance loss.

$$R(t) = \frac{S^{Margin}(t) - S^{Loss}(t)}{S^{Margin}(t)}, \tag{23}$$

where $R(t)$ indicates the resilience of the metro network, and its value range is [0,1]. The larger the $R(t)$ value, the better the network performance; the closer the value is to 1, the better the recovery during the recovery stage. $S^{Margin}(t) - S^{Loss}(t)$ indicates the actual performance maintained, i.e., the actual performance level that the system can maintain in the face of external attacks, which is the ability to maintain the normal operation of the system.

4. Emergency Maintenance of Urban Metro System for Resilience Enhancement

When urban metro systems experience emergencies or localized failures, implementing emergency maintenance on the affected stations is critical for enhancing system resilience. However, due to limitations in manpower, materials, equipment, and other resources, it is often impractical to maintain all failed stations simultaneously. Therefore, under resource-constrained conditions, developing a well-designed recovery strategy to determine the priority of station restoration can significantly improve the effectiveness of emergency maintenance and the efficiency of resilience enhancement.

Different recovery strategies evaluate node importance from various structural or functional dimensions of the system, thereby providing a basis for determining the priority of recovery sequences. Common node recovery strategies include betweenness-based recovery strategy (BBRS), degree-based recovery strategy (DBRS), eigenvector centrality-based recovery strategy (ECBRS), revenue growth-based recovery strategy (RGBRS).

These strategies enhance the resilience of the metro network from diverse perspectives. Based on the concept of resilience, this paper proposes a cost importance-based recovery strategy (CIBRS), i.e., nodes are sorted based on their importance, and the nodes with high importance are recovered first. In this section, the cost importance of a node is defined as the performance increase per unit time during the recovery stage, and the cost importance I_{∂}^{C} of the failed node S_{∂} can be expressed as

$$I_{\partial}^{C} = \frac{\Delta P_{\partial}}{\Delta t_{\partial}} = \frac{P\left(t_{\partial}^{recovery}\right) - P\left(t_{\partial-1}^{recovery}\right)}{t_{\partial}^{recovery} - t_{\partial-1}^{recovery}}. \tag{24}$$

The CIBRS integrates both the node performance enhancement and recovery time, prioritizing nodes that can achieve higher performance gains with lower time under limited resources. In a metro network, the cost importance of different nodes is different. The higher the importance, the more critical the node is, and the greater the contribution to the resilience enhancement after recovering that node. For two neighboring nodes S_p and S_q in the recovery sequence, let I_p^C and I_q^C denote the cost importance of S_p and S_q, respectively. According to **Eq. (25)**, we obtain $I_p^C = \frac{\Delta P_p}{\Delta t_p} = \frac{P(t_p^{recovery}) - P\left(t_{p-1}^{recovery}\right)}{t_p^{recovery} - t_{p-1}^{recovery}}$ and $I_q^C = \frac{\Delta P_q}{\Delta t_q} = \frac{P(t_q^{recovery}) - P\left(t_{q-1}^{recovery}\right)}{t_q^{recovery} - t_{q-1}^{recovery}}$. If $I_p^C > I_q^C$, it can be obtained

$$\Delta P_p \cdot \Delta t_q > \Delta P_q \cdot \Delta t_p. \tag{25}$$

The overall resilience of the metro system is the ability to resist, adapt, and absorb the impact of attacks, including the normal, failure evolution, and recovery stages. Therefore, the resilience of the entire process can be taken at time $t = t_w^{recovery}$,

$$R(t) = \frac{1}{[P_{Nor} - P(t_u^{failure})](t_w^{recovery} - t_0^{failure})} \left\{ \begin{array}{c} [P_{Nor} - P(t_u^{failure})](t_w^{recovery} - t_0^{failure}) \\ -\left\{ \sum_{\theta=1}^{u-1} [P(t_{\theta-1}^{failure}) - P(t_{\theta}^{failure})](t - t_{\theta}^{failure}) + \sum_{\partial=1}^{w} [P_{Nor} - P(t_{\partial-1}^{recovery})](t_{\partial}^{recovery} - t_{\partial-1}^{recovery}) \right\} \end{array} \right\}. \tag{26}$$

$R_{p\to q}$ is the resilience value of the network when recovering S_p first and then S_q, and $R_{q\to p}$ is the resilience value of the network when recovering S_q first and then S_p. The failure evolution process under different strategies is the same. However, the recovery stage differs (**Fig. 7 and Fig. 8**). Therefore, the comparison of resilience only considers the differences ΔS^{ID} in indirect costs brought about by different node recovery sequences during the recovery stage. Let $S_{p\to q}^{ID}$ indicate the increase in indirect costs brought by recovering S_p first and then S_q, and let $\Delta S_{q\to p}^{ID}$ indicate the increase in indirect costs brought by recovering S_q first and then S_p, we have

$$\Delta S_{p\to q}^{ID} = \Delta t_p \cdot \left(\Delta P_p + \Delta P_q\right) + \Delta t_q \cdot \Delta P_q, \tag{27}$$

$$\Delta S_{q\to p}^{ID} = \Delta t_q \cdot \left(\Delta P_p + \Delta P_q\right) + \Delta t_p \cdot \Delta P_p. \tag{28}$$

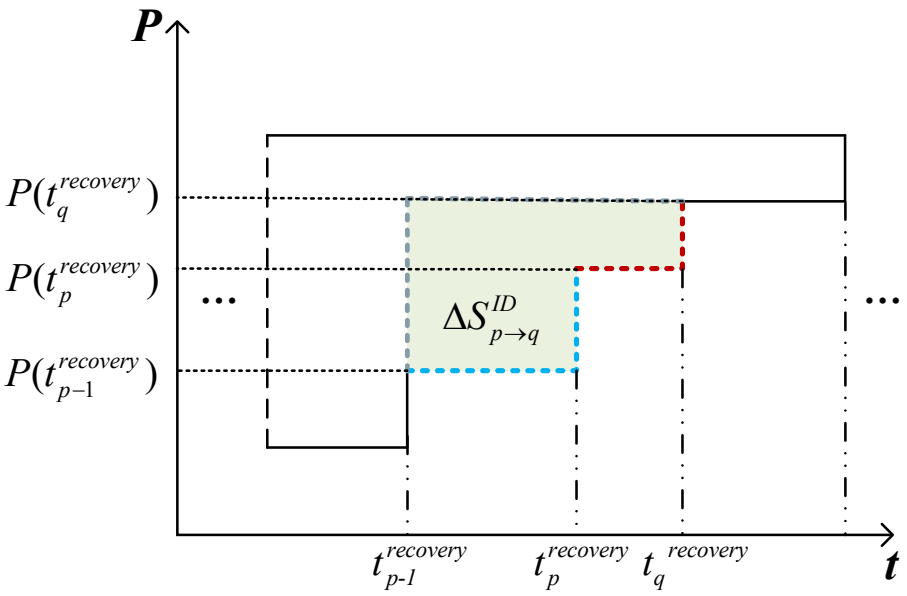


Fig. 7. Performance change when recovering S_p first and then S_q ($\boldsymbol{t_{q-1}^{recovery} = t_p^{recovery}}$)

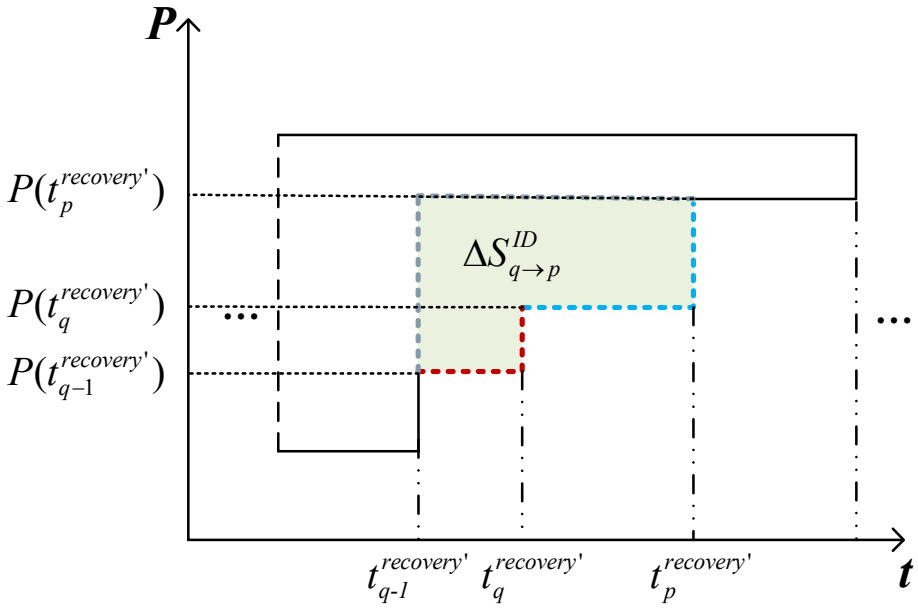


Fig. 8. Performance change when recovering S_q first and then S_p ($\boldsymbol{t_{p-1}^{recovery'} = t_q^{recovery'}}$)

Combining **Eq. (27)** and **Eq. (28)**, it is obtained $S_{q\to p}^{ID} - S_{p\to q}^{ID} = \Delta P_p \cdot \Delta t_q - \Delta P_q \cdot \Delta t_p$. Based on **Eq. (25)**, it is obtained that $\Delta S_{q\to p}^{ID} - \Delta S_{p\to q}^{ID} > 0$, i.e. $R_{p\to q} > R_{q\to p}$. Therefore, if $I_p^C > I_q^C$, S_p should be recovered first, and the resilience value of the network will be higher at this time; on the contrary, if $I_p^C < I_q^C$, S_q should be recovered first. Determining the recovery sequence based on the nodes' cost importance can enhance system resilience more effectively.

5. Case study

5.1 Data Source

This paper selected the Beijing metro in China (https://www.bjmetro.com) for the case study. The Beijing metro started trial operation on January 15, 1971. Until December 2022, there are 23 lines in operation in Beijing (excluding suburban railways), with an annual vehicle mileage of 6880.08 million kilometers and an annual passenger volume of 2.26 billion person-times, with a daily average passenger volume of 6.201 million person-times.

Based on the location of Beijing metro lines and stations, and referring to the "2023 Beijing Transportation Development Annual Report", the number of stations and average passenger flow on weekdays of each metro line were obtained. This study selected 17 lines and 339 stations for analysis. The distribution of each line and station is shown in **Fig. 9** (nodes are no longer renumbered, and the first numbering is used as the standard), and the number of stations and passenger flow are shown in **Table 1**.

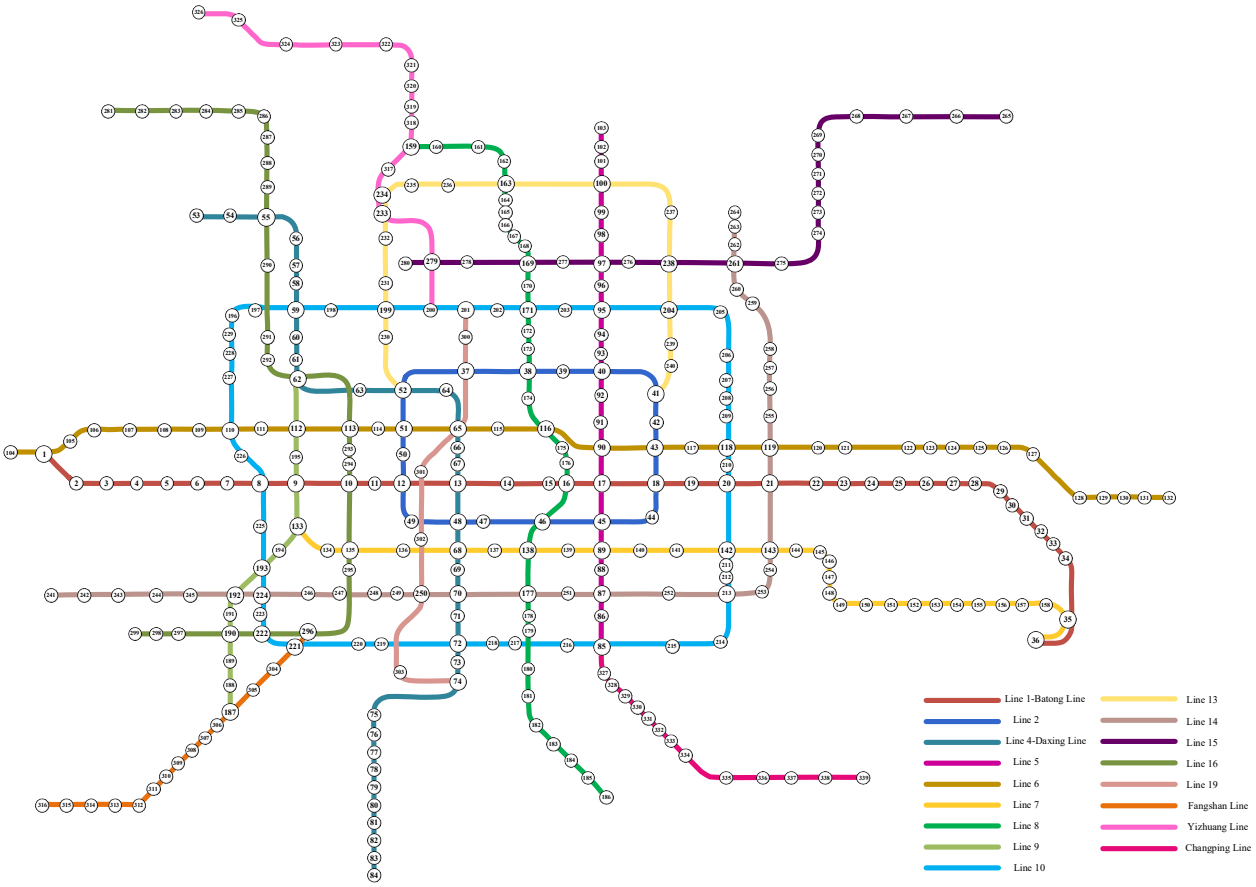


Fig. 9. The network topology of Beijing metro

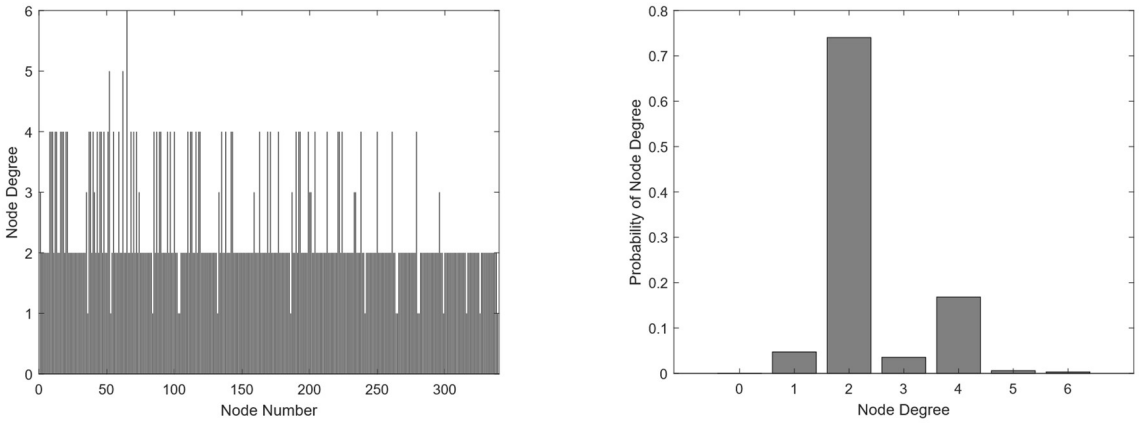
Table 1. Beijing metro stations and passenger flow

Line	Station	Average daily passenger flow on weekdays(ten thousand passengers)
Line 1-Batong Line	36	66.01
Line 2	18	47.67
Line 4-Daxing Line	35	67.45
Line 5	22	60.5
Line 6	34	70
Line 7	30	34.94
Line 8	33	39.4
Line 9	13	31.45
Line 10	45	113.22
Line 13	17	44.56
Line 14	33	53.41
Line 15	20	29.36
Line 16	26	12.17
Line 19	9	6.3
Fangshan Line	16	19.92
Changping Line	15	17.91
Yizhuang Line	14	15.83

Based on the connection status of nodes in **Fig. 9**, the adjacency matrix of the Beijing metro network is established. The size of the adjacency matrix is 339*339, and its values are

$$A = \begin{bmatrix} a_{1,1} & a_{1,2} & \dots & a_{1,339} \\ a_{2,1} & a_{2,2} & \dots & a_{2,339} \\ \vdots & \vdots & \ddots & \vdots \\ a_{339,1} & a_{339,2} & \dots & a_{339,339} \end{bmatrix}.$$

The degree and distribution of the Beijing metro network nodes are obtained using the adjacency matrix (**Fig.10**).



(a) Degree values of each node (b) Node degree distribution

Fig. 10. Degree and distribution of the Beijing metro network nodes

In the Beijing metro network, the maximum node degree is 6, and the minimum is 1. Most of the nodes in the

network have a degree of 2. Nodes with a degree of 6 are only S_{65}. Nodes with a degree of 1 indicate that there is one station connected, which is generally the starting station or the terminal station, accounting for about 4.72% of the total number of stations; nodes with a degree of 2 indicate that there are two stations connected, which are intermediate stations in the line, accounting for about 74.04% of the total number of stations; nodes with a degree of 3 account for 3.54%, and nodes with a degree of 4 account for 16.81%. Nodes with a degree more than 2 are connected to multiple stations and are transfer stations, accounting for 21.24% of the total number of stations.

5.2 Result Simulation

The cascading failure range caused by attacking different nodes varies. During the morning and evening peak hours, the maximum section load factor of certain line sections is too high, which can lead to failures in those sections. By analyzing the maximum section load factor of the Beijing metro network, lines with high load are selected for study. Line sections with a maximum section load factor exceeding 100% are shown in **Table 2**.

Table 2. Beijing metro line sections with a **maximum section load factor** exceeding 100%

Affiliated Line	Occurring Section	Maximum Section Load Factor	Maximum Section Passenger Flow (100,000 person-times/hour)
Line 4-Daxing Line	Caishi Kou-Xuanwu Men	118%	5.48
Line 5	Huixin Xijie Beikou-Huixin Xijie Nankou	104%	4.43
Line 15	Cuigezhuang-Wangjing Xi (E)	104%	2.89
Line 10	Shuangjing-Guomao	100%	4.99

The following process is used to attack the Beijing metro network:

Steps 1: Obtain the average daily passenger flow of the Beijing metro for the workdays of 2022 based on the annual report data, construct the initial load matrix, and calculate the income of the Beijing metro under normal conditions.

Steps 2: Select an appropriate tolerance parameter and, based on **Eq. (1)**, calculate the capacity of each node and obtain the capacity matrix of the Beijing metro network.

Steps 3: Identify the line sections prone to failure based on the maximum section load factor and assume failure. The failure will cause the starting station of the section to have an increased passenger flow, become overloaded, and fail. The number of failed nodes in the network increases by 1.

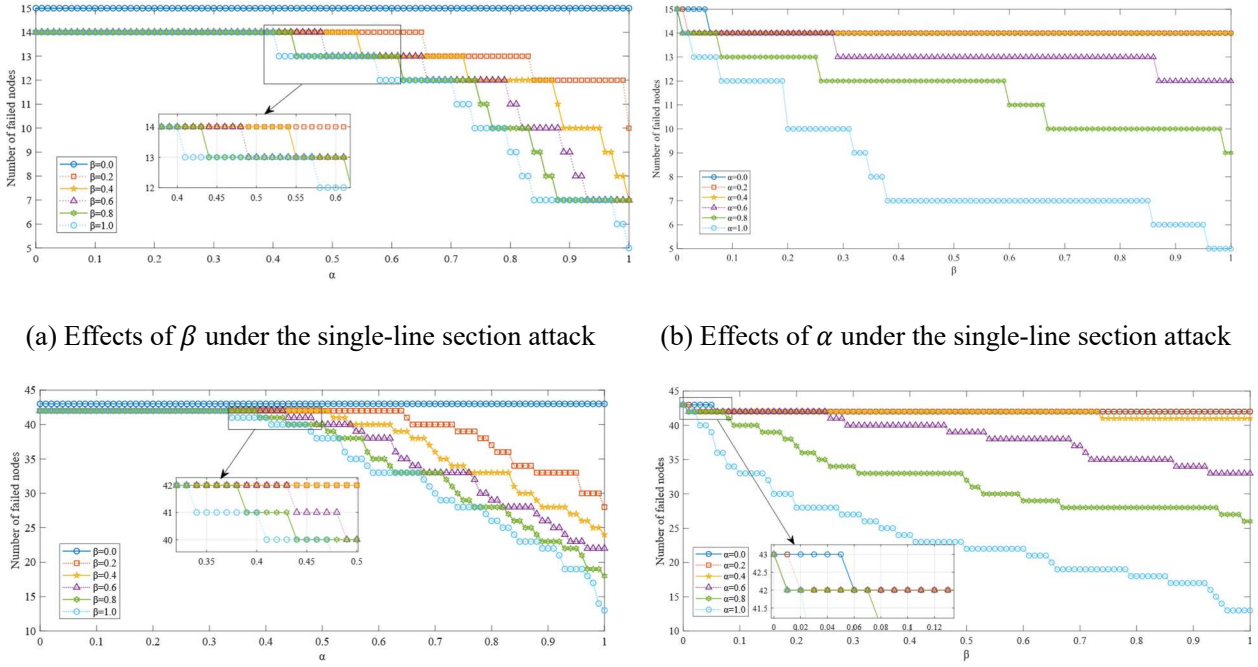
Steps 4: Use the adjacency matrix to find the neighboring nodes of the failed node. The load exceeding the capacity of the failed node is transferred or leaves based on **Eq. (3)** and **Eq. (4)**. Currently, the load of the failed node in the load matrix becomes its capacity, and the load of the neighboring nodes increases; the connection status between the failed node and the neighboring nodes in the adjacency matrix becomes 0, i.e., the failed node no longer accepts

secondary load distribution. Calculate the income of the metro system at this time based on the updated load.

Steps 5: Compare the load and capacity of each node after the update. When a node's load exceeds its capacity, that node fails, and the number of failed nodes increases. Similarly, the load of the failed node is distributed based on step 4.

Repeat steps 4 and 5. When the load of all nodes in the network does not exceed the capacity, the cascading failure ends.

The scale of the failure is often related to the number and location of the initial failed nodes. Based on the above maximum section load factor, this paper analyses two attack scenarios: a single-line section attack and a multi-line section attack. For the single-line section attack scenario, the study selects the section with the highest load factor (Caishi Kou-Xuanwu Men). For the multi-line section attack scenario, the study selects sections with a load factor exceeding 100% and a high passenger flow (Caishi Kou-Xuanwu Men, Huixin Xijie Beikou-Huixin Xijie Nankou, and Shuangjing-Guomao). Based on these scenarios, we analyse the relationship between tolerance parameters and the number of failed nodes, as shown in **Fig. 11**.



(a) Effects of β under the single-line section attack

(b) Effects of α under the single-line section attack

(c) Effects of β under the multi-line section attack

(d) Effects of α under the multi-line section attack

Fig. 11. Effects of tolerance parameters (α and β) on the number of failed nodes under different attack scenarios

Fig. 11 shows the impact of changes in tolerance parameters (α and β) on the number of failed nodes under both single-point and multi-point attack scenarios, consisting of four subplots: (a) and (b) represent the effects of adjusting β and α under the single-line section attack scenario, while (c) and (d) correspond to the results under the multi-line section attack scenario. Based on the overall trends and key details in **Fig. 11**, the following analyses

can be made: (1) From the overall trend, the number of failed nodes decreases with the increase of α or β, indicating that higher tolerance parameters contribute to improved system robustness. This is because the increase in α or β directly enhances the capacity of stations in the metro network, strengthening the nodes' ability to resist attacks, thereby suppressing the spread of cascading failures and ultimately reducing the failure scale. This verifies the positive correlation between parameters and network resilience. (2) Subplots (a) and (c) show that as β increases, the adjustment effect of α becomes stronger, as indicated by the increasing slope of each curve. Similarly, subplots (b) and (d) also show that the higher β is, the stronger the adjustment ability of α. This suggests that with the increase of one parameter, the sensitivity of the other parameter's adjustment improves, indicating a positive coupling relationship between α and β. (3) Taking the curve with α=0.8 in (d) as an example, when β is in the range of 0.67 to 0.78, the number of failed nodes stabilizes at 19 and no longer decreases with the increase of β. This result reveals the marginal effect of parameter optimization: when α=0.8 and β=0.67, the network has reached a saturation status within this range. Continuing to invest resources to increase β does not produce additional benefits, leading to resource redundancy. (4) Comparing (c) and (d), it can be found that there are significant differences in the adjustment costs of α and β to achieve the same reduction in the number of failed nodes. For example, when the system's initial status is α=0.6 and β=0.6, to reduce the number of failed nodes from 38 to 34: with β fixed at 0.6, α needs to be increased by 0.06; while with α fixed at 0.6, β needs to be increased by 0.27. Operational management departments can compare the resource investment costs of different solutions and prioritize the parameters with higher adjustment efficiency, thus formulating more cost-effective network optimization strategies to maximize resource utilization efficiency.

Based on the influence of the tolerance parameters α and β on the number of failed nodes, this paper selects a set of fixed tolerance parameters (α=0.8, β=0.6) to further explore the failure process and development characteristics of the metro network under the single-line section attack and multi-line section attack scenarios, providing a basis for the subsequent evaluation and comparison of the applicability and effectiveness of different recovery strategies.

Due to the varying distances between neighboring stations, the travel time of each train on different line sections differs. According to statistics, the travel time between neighboring stations on the Beijing metro is mostly between 3 to 6 minutes. Since the cascading failure process is the same under different recovery strategies and does not have an absolute impact on the evaluation results, this paper assumes that the transfer time between neighboring stations is 5 minutes. Additionally, trains arriving in different directions are considered to reach at the same time, meaning that every five minutes, a train will transfer passengers to a neighboring station of the failed

station. **Fig. 12** and **Fig. 13** show the cascading failure scale under single-line and three-section attack scenarios, respectively.

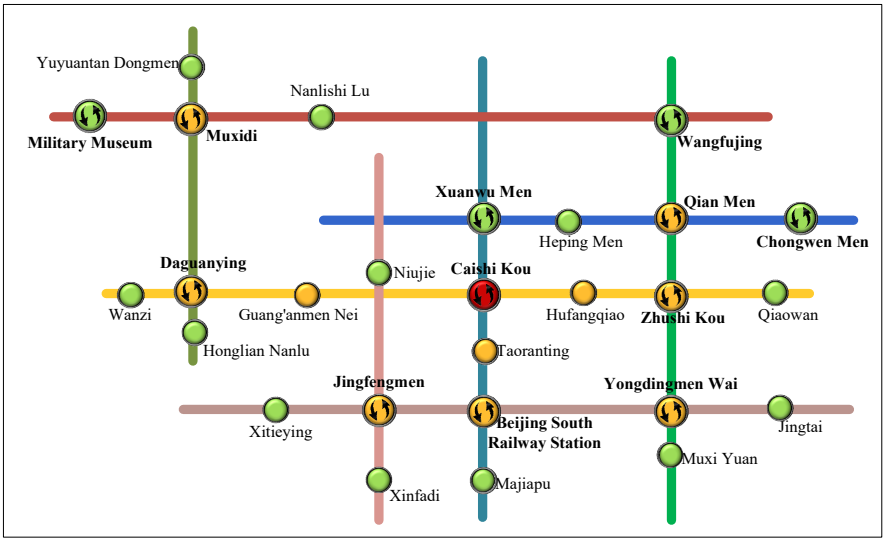


Fig. 12. Cascading failure nodes caused by a single-line section attack

It can be seen from **Fig. 12** that initially, the section from the Caishi Kou station to the Xuanwu Men Station is disturbed, and many passengers are stranded at the Caishi Kou station. $t_1^{failure} = 5$, 68-Caishi Kou fails; $t_2^{failure} = 10$, 69-Taoranting, 136-Guang'anmen Nei and 137-Hufangqiao fail; $t_3^{failure} = 15$, 70-Beijing South Railway Station, 135-Daguanying and 138-Zhushikuo fail; $t_4^{failure} = 20$, 10-Muxidi, 46-Qianmen, 177-Yongdingmen Wai and 250-Jingfengmen fail.

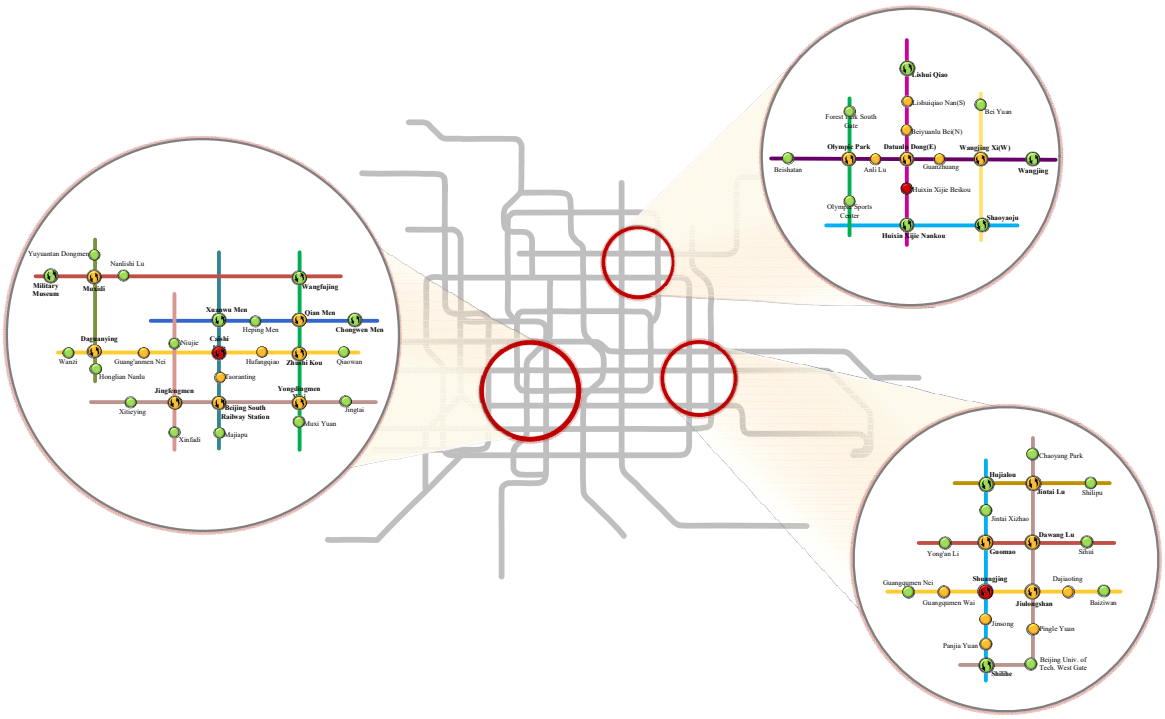


Fig. 13. Cascading failure nodes caused by a three-line section attack

From **Fig. 13**, the initial failed stations are 68-Caishi Kou, 142-Shuangjing, 96-Huixinxijie Beikou at $t_1^{failure} = 5$. $t_2^{failure} = 10$, 69-Taoranting, 97-Datunlu Dong (E), 136-Guang'anmen Nei, 137-Hufangqiao, 141-Guangqumen Wai, 143-Jiulongshan and 211-Jinsong fail; $t_3^{failure} = 15$, 21-Dawang Lu, 70-Beijing South Railway Station, 98-Beiyuanlu Bei (N), 135-Daguanying, 138-Zhushi Kou, 144-Dajiaoting, 212-Panjia Yuan, 254-Pingle Yuan, 276-Guanzhuang and 277-Anli Lu fail; $t_4^{failure} = 20$, 10-Muxidi, 20-Guomao, 46-Qian Men, 99-Lishuiqiao Nan (S), 119-Jintai Lu, 169-Olympic Park, 177-Yongdingmen Wai, 238-Wangjing Xi (W) and 250-Jingfengmen fail.

The larger the scale of the station, the more complex the recovery stage. Therefore, it is assumed that the recovery time is proportional to the station capacity, and based on past experience, the recovery time $t_\partial^{recovery} = Q_\partial/100$ is taken. The emergency maintenance effect of the metro network largely depends on the recovery strategy, and a good recovery sequence can better enhance the network resilience. When the node recovery sequence is the same under the same strategy, the node with a higher performance enhancement recovery value should be selected for recovery first. Based on the above assumptions, five recovery strategies are applied to enhance the performance of the metro system after failure, resulting in recovery outcomes for both single-line and multi-line section attack scenarios.

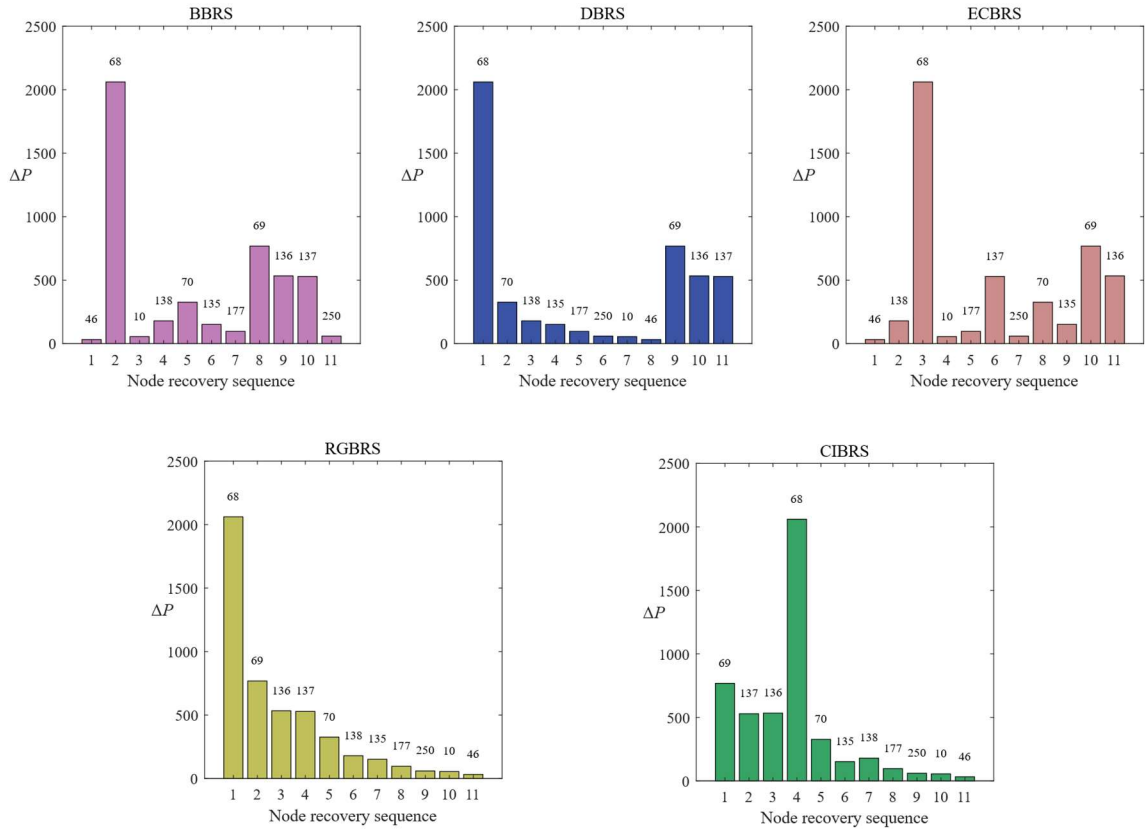


Fig. 14. Node recovery sequence under the single-line section attack scenario with different strategies

Fig. 14 shows the impact of node recovery sequence on performance enhancement under different recovery strategies for single-line section failure. Based on the recovery rules of the five strategies, the recovery sequence of BBRS is 46-68-10-138-70-135-177-69-136-137-250, the recovery sequence of DBRS is 68-70-138-135-177-250-10-46-69-136-137, the recovery sequence of ECBRS is 46-138-68-10-177-137-250-70-135-69-136, the recovery sequence of RGBRS is 68-69-136-137-70-138-135-177-250-10-46, and the recovery sequence of CIBRS is 69-137-136-68-70-135-138-177-250-10-46.

Based on the above node recovery sequence and recovery time, the variation of metro network performance over time is shown in **Fig. 15**.

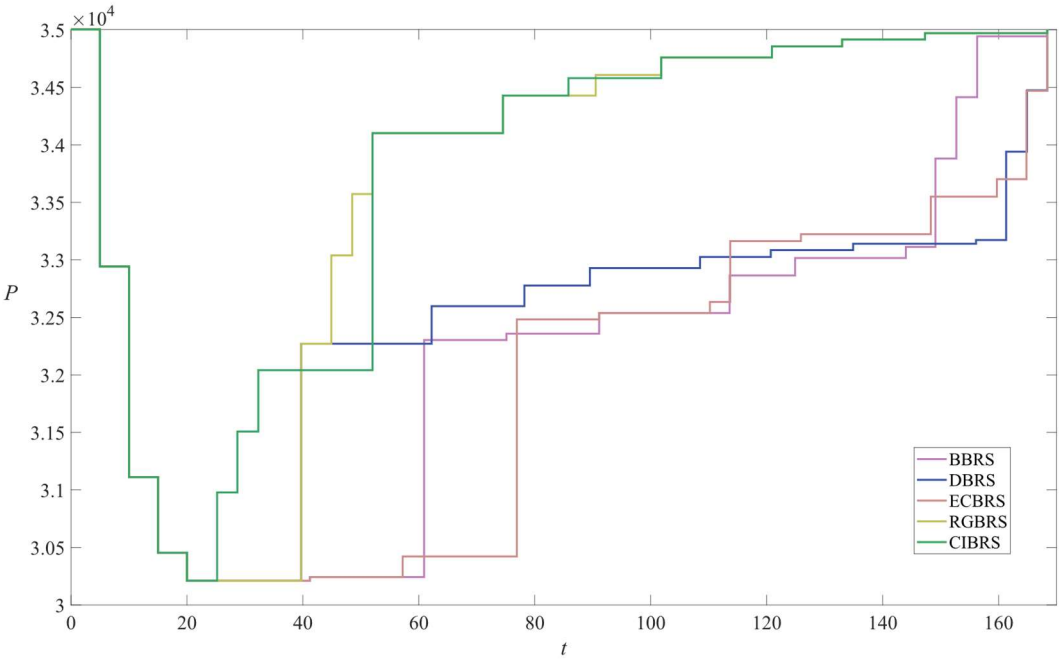


Fig. 15. Performance changes of five recovery strategies under the single-line section attack scenario

It can be seen from **Fig.15** that all recovery strategies show a positive impact on network performance. Based on Figs 14 and 15, it can be observed that S_{68} provides the greatest performance enhancement to the system, with performance enhancements occurring at $t = 60.9$, $t = 39.7$, $t = 76.9$, $t = 39.7$, and $t = 52$ under the five strategies, respectively. Additionally, by observing the distribution of high-performance enhancement nodes, it can be seen that in DBRS, high-performance enhancement nodes are concentrated at the beginning and end, with a performance recovery peak appearing again at the ninth recovery node (S_{69}). This indicates that, although S_{69} has a lower degree, its connection with S_{68}, which has a higher degree and a larger passenger flow recovery, leads to a higher passenger flow passing through S_{69}, resulting in a more significant performance enhancement compared to other nodes with similar degrees. In RGBRS and CIBRS, high-performance enhancement nodes are concentrated earlier, and in CIBRS, the highest performance enhancement occurs at S_{68} in the fourth recovery,

suggesting that the performance enhancement efficiency of S_{68} is lower than that of S_{69}, S_{137}, and S_{136}. In BBRS and ECBRS, high-performance enhancement nodes are more scattered; while some nodes have a higher global influence and play a key role in recovering network connectivity, their own passenger flow recovery is relatively small. From the perspective of recovery time, system performance under CIBRS and RGBRS is rapidly recovered in the early stages, but the recovery speed gradually slows down as the process progresses. For the other three strategies, the recovery speed initially slows down and then accelerates.

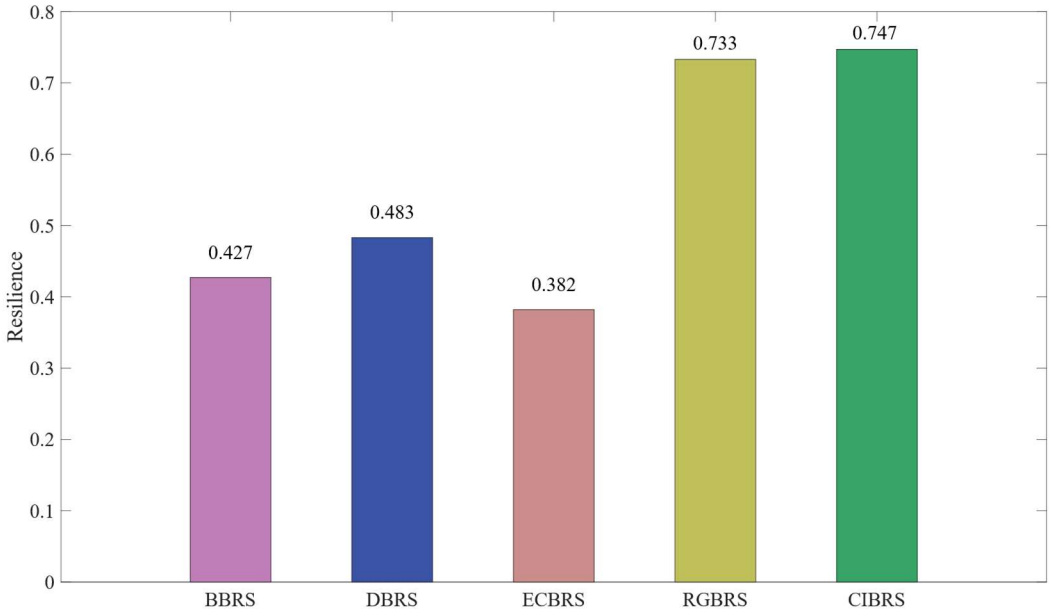


Fig. 16. Resilience value achieved by five recovery strategies under the single-line section attack scenario

By calculation, the BBRS can enhance the system resilience to 0.427, the DBRS can enhance the system resilience to 0.483, the ECBRS can enhance the system resilience to 0.382, the RGBRS can enhance the system resilience to 0.733, and the CIBRS can enhance the system resilience to 0.747. The five strategies are ranked in terms of resilience: CIBRS>RGBRS>DBRS>BBRS>ECBRS.

Figs. 14-16 present the node recovery sequence, system performance changes, and resilience comparison under five recovery strategies in the single-line section attack scenario. Based on this, the recovery process in the multi-line section attack scenario is analysed, further exploring the applicability of different recovery strategies in complex scenarios.

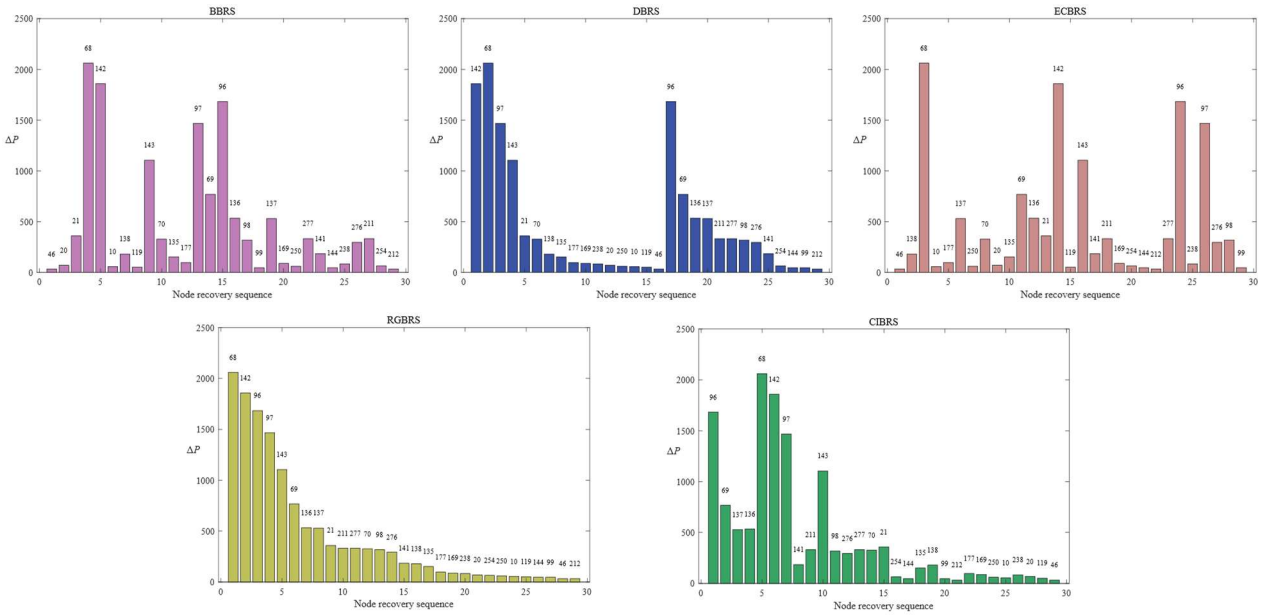


Fig. 17. Node recovery sequence under the multi-line section attack scenario with different strategies

From **Fig. 17**, the recovery sequence of BBRS is 46-20-21-68-142-10-138-119-143-70-135-177-97-69-96-136-98-99-137-169-250-277-141-144-238-276-211-254-21, the recovery sequence of DBRS is 142-68-97-143-21-70-138-135-177-169-238-20-250-10-119-46-96-69-136-137-211-277-98-276-141-254-144-99-212, the recovery sequence of ECBRS is 46-138-68-10-177-137-250-70-20-135-69-136-21-142-119-143-141-211-169-254-144-212-277-96-238-97-276-98-99, the recovery sequence of RGBRS is 68-142-96-97-143-69-136-137-21-211-277-70-98-276-141-138-135-177-169-238-20-254-250-10-119-144-99-46-212, and the recovery sequence of CIBRS is 96-69-137-136-68-142-97-141-211-143-98-276-277-70-21-254-144-135-138-99-212-177-169-250-10-238-20-119-46.

Based on the above node recovery sequence and recovery time, the variation of metro network performance over time is shown in **Fig. 18**.

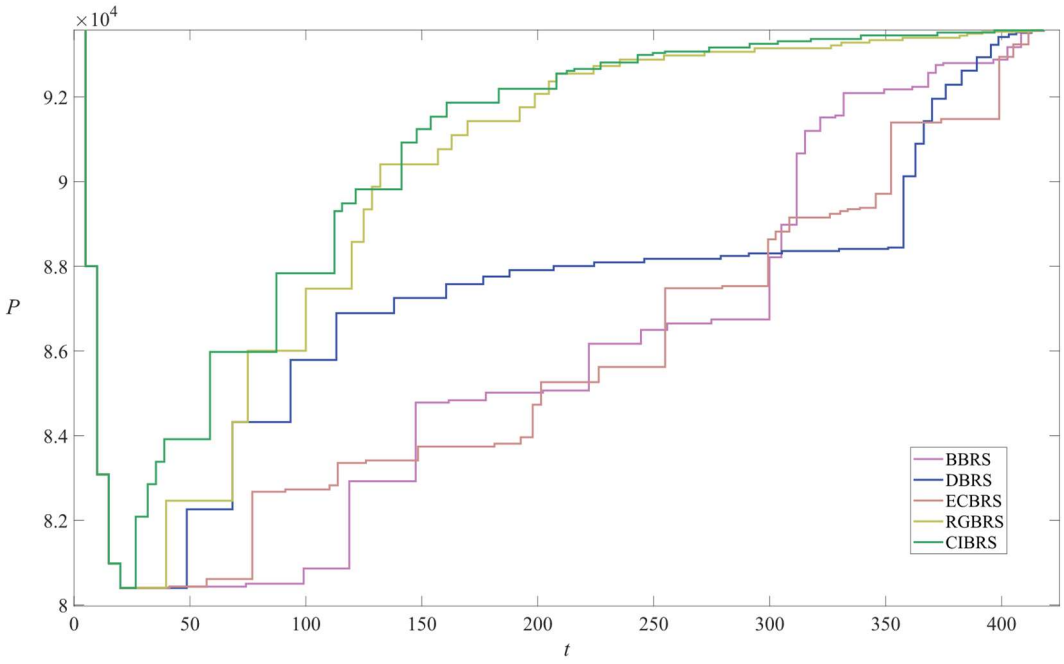


Fig. 18. Performance changes of five recovery strategies under the multi-line section attack scenario

Compared to **Fig. 15**, the differences in the performance recovery process under the five strategies are more significant in the multi-line section attack scenario in **Fig. 18**. From **Figs. 17 and 18**, it can be seen that S_{68} provides the greatest performance enhancement, with enhancements appearing at $t = 118.7$, $t = 68.33$, $t = 76.87$, $t = 39.7$, and $t = 58.63$ under the five strategies, respectively. The distribution of the recovery sequence for high-performance enhancement nodes exhibits similar characteristics to the single-line section attack scenario. It is worth noting that in **Fig. 18**, CIBRS has the fastest recovery speed, followed by RGBRS. Under these two strategies, the system performance is rapidly recovered in the early stages. The recovery speed of DBRS is better than that of BBRS and ECBRS in the early stage, but as the recovery progresses, the speed slows down significantly. At $t = 305.03$, the performance under DBRS falls below that of the other four strategies, and only at $t = 357.67$ does the recovery speed increase. The recovery speeds of BBRS and ECBRS alternate between fast and slow.

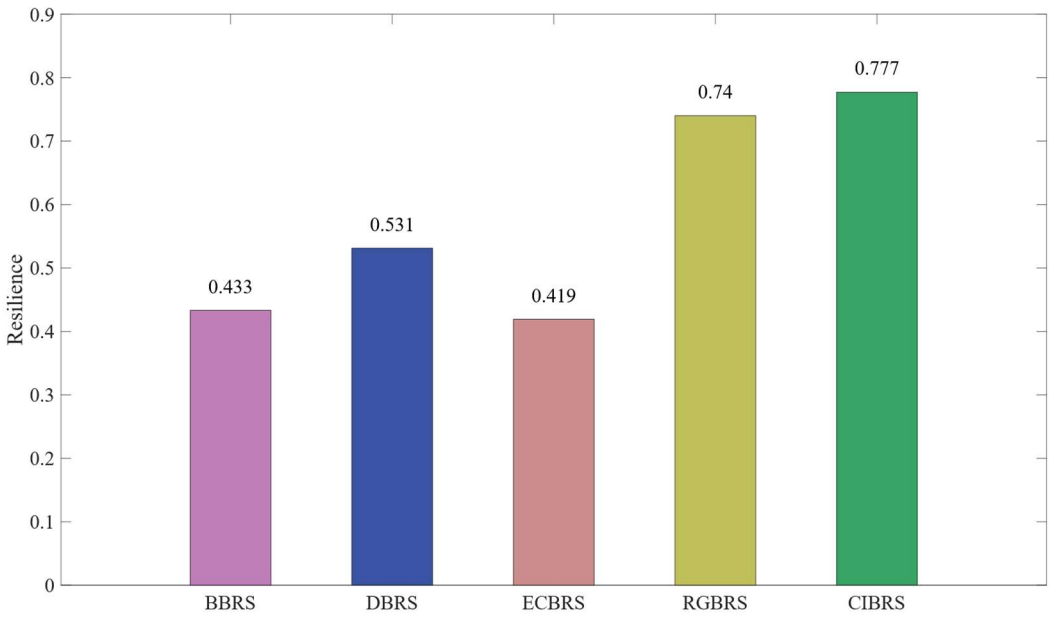


Fig. 19. Resilience value achieved by five recovery strategies under the multi-line section attack scenario

By calculation, the BBRS can enhance the system resilience to 0.433, the DBRS can enhance the system resilience to 0.531, the ECBRS can enhance the system resilience to 0.419, the RGBRS can enhance the system resilience to 0.740, and the CIBRS can enhance the system resilience to 0.777. The five strategies are ranked in terms of resilience: CIBRS>RGBRS>DBRS>BBRS>ECBRS.

By comparing the recovery processes in the single-line section attack scenario (**Figs 14-16**) and the multi-line section attack scenario (**Figs 17-19**), the following findings can be made: (1) In both attack scenarios, the distribution of high-performance nodes under the five recovery strategies shows similar patterns. The strategies (BBRS, DBRS, ECBRS) prioritize nodes that play an important role in the network structure, while the last two strategies (RGBRS, CIBRS) focus more on improving the system's functionality to enhance economic benefits and service levels. (2) In both attack scenarios, the effectiveness ranking of recovery strategies is the same, indicating the stability of their effects during the recovery process. Furthermore, the CIBRS maintains a high resilience enhancement effect across different attack scenarios, demonstrating good adaptability and stability. In the single-line section attack scenario, the CIBRS improves resilience by 74.94%, 35.34%, 95.55%, and 1.91% compared to BBRS, DBRS, ECBRS, and RGBRS, respectively. In the multi-line section attack scenario, CIBRS improves resilience by 79.45%, 46.33%, 85.44%, and 5.00% compared to BBRS, DBRS, ECBRS, and RGBRS, respectively. This strategy has good adaptability and robustness, and the resilience enhancement effect under multi-line section attacks is more significant.

6. Conclusions and future work

To address the challenge of system recovery in complex metro networks following attacks, this study introduces a resilience evaluation method and emergency maintenance strategy based on DT and generative AI. In the model formulation, the cost impacts induced by passenger flow variations during the failure and recovery stages are considered, and the role of tolerance parameters in mitigating cascading failures is examined, providing theoretical support for the design and regulation of real-world metro systems. Additionally, a recovery strategy based on cost importance is proposed to guide emergency maintenance optimization under limited resource. Compared with other strategies (BBRS, DBRS, ECBRS, RGBRS), the proposed recovery strategy improves system resilience by 74.94%, 35.34%, 95.55%, and 1.91% under the single-line section attack scenario, and by 79.45%, 46.33%, 85.44%, and 5.00% under the multi-line section attack scenario, respectively. This indicates that the strategy has better adaptability and practical significance under complex conditions.

However, there are still some spaces to be further studied. For example, this study does not consider intermodal transportation systems, passenger travel demand and dynamic recovery process. At the same time, the metro revenue comes from multiple sources. In future work, more variables and scenarios will be considered further to optimize the proposed resilience evaluation model of the metro network. Additionally, we will consider the interdependence between the metro system and other public transportation modes, as well as the coupling relationship between nodes during the recovery process.

Acknowledgments

The authors gratefully acknowledge the financial support for this research from the Natural Science Foundation of Henan Province (No. 252300421005).

References

[1] Dui H, Zhang H, Dong X, Wu S, Wang Y. Multi-Stage Control Strategy of IoT-Enabled Unmanned Vehicle Detection Systems. IEEE Trans Intell Transport Syst 2025, DOI: 10.1109/TITS.2025.3535737.

[2] Yuan H, He Y, Zhou J, Li Y, Cui X, Shen Z. Research on compactness ratio model of urban underground space and compact development mechanism of rail transit station affected area. Sustainable Cities Soc 2020;55:102043.

[3] Dui H, Zhang Y, Xing L. Dynamic reliability assessment model for IoT-enabled smart offshore wind farm. IEEE Transactions on Reliability, 2024, DOI: 10.1109/TR.2024.3428870.

[4] Qiao Y, Peng F, Sabri S, Rajabifard A. Low carbon effects of urban underground space. Sustainable Cities Soc 2019;45:451–9.

[5] Du B, Du H, Liu H, Niyato D, Xin P, Yu J, et al. YOLO-Based Semantic Communication With Generative AI-

Aided Resource Allocation for Digital Twins Construction. IEEE Internet Things J 2024;11:7664–78.
[6] Xia M, Shao H, Williams D, Lu S, Shu L, de Silva CW. Intelligent fault diagnosis of machinery using digital twin-assisted deep transfer learning. Reliab Eng Syst Saf 2021;215:107938.
[7] Zio E, Miqueles L. Digital twins in safety analysis, risk assessment and emergency management. Reliab Eng Syst Saf 2024;246:110040.
[8] Dui H, Zeng Q, Xie M. Generative AI-based spatiotemporal resilience, green and low-carbon transformation strategy of smart renewable energy systems. Front Eng Manag, 2025, DOI: 10.1007/s42524-025-4147-6.
[9] Wang L, Deng T, Shen Z-JM, Hu H, Qi Y. Digital twin-driven smart supply chain. Front Eng Manag 2022;9:56–70.
[10] Dui H, Li H, Wu S. Performance analysis of IoT-enabled hydro-photovoltaic power systems considering electrical power mission chains. Energy Conversion and Management, 2024; 319, 118962.
[11] Shao X, Cai B, Zou Z, Shao H, Yang C, Liu Y. Artificial intelligence enhanced fault prediction with industrial incomplete information. Mech Syst Sig Process 2025;224:112063.
[12] Shao X, Cai B, Gao L, Zhang Y, Yang C, Gao C. Data-model-linked remaining useful life prediction method with small sample data: A case of subsea valve. Reliab Eng Syst Saf 2024;250:110323.
[13] Cai B, Shao X, Liu Y, Kong X, Wang H, Xu H, et al. Remaining Useful Life Estimation of Structure Systems Under the Influence of Multiple Causes: Subsea Pipelines as a Case Study. IEEE Trans Ind Electron 2020;67:5737–47.
[14] Cai B, Fan H, Shao X, Liu Y, Liu G, Liu Z, et al. Remaining useful life re-prediction methodology based on Wiener process: Subsea Christmas tree system as a case study. Comput Ind Eng 2021;151:106983.
[15] Huang X, Yang H, Zhou C, He M, Shen X, Zhuang W. When Digital Twin Meets Generative AI: Intelligent Closed-Loop Network Management. IEEE Network 2024:1–1.
[16] Mata O, Ponce P, Perez C, Ramirez M, Anthony B, Russel B, et al. Digital twin designs with generative AI: crafting a comprehensive framework for manufacturing systems. J INTELL MANUF 2025:1-24.
[17] Chen C, Shi J, Lu N, Zhu ZH, Jiang B. Data-driven predictive maintenance strategy considering the uncertainty in remaining useful life prediction. Neurocomputing 2022;494:79–88.
[18] Li M, Jiang X, Carroll J, Negenborn RR. A multi-objective maintenance strategy optimization framework for offshore wind farms considering uncertainty. Appl Energy 2022;321:119284.
[19] Dui H, Lu Y, Gao Z, Xing L. Performance efficiency and cost analysis of multi-state systems with successive damage and maintenance in multiple shock events. Reliab Eng Syst Saf 2023;238:109403.
[20] Han K, Zhang D, Chen X, Su D, Ju J-WW, Lin X, et al. A resilience assessment framework for existing underground structures under adjacent construction disturbance. Tunnelling Underground Space Technol 2023;141:105339.
[21] Xu P, Lu Q, Feng T, Li J, Li G, Xu X. Resilience analysis of metro stations integrating infrastructures and passengers. Reliab Eng Syst Saf 2024;252:110467.
[22] Lu Q, Li J, Xu P, Zhang L, Cui X. Modeling cascading failures of urban rail transit network based on passenger spatiotemporal heterogeneity. Reliab Eng Syst Saf 2024;242:109726.
[23] Dui H, Zhang H, Dong X, Zhang S. Cascading failure and resilience optimization of unmanned vehicle distribution networks in IoT. Reliab Eng Syst Saf 2024;246:110071.
[24] Cai B, Kong X, Liu Y, Lin J, Yuan X, Xu H, et al. Application of Bayesian Networks in Reliability Evaluation.

IEEE Trans Ind Inf 2019;15:2146–57.
[25] Chen J, Liu X, Du B, Li W, Yin Y, Xu X. Passenger-oriented resilience assessment of an urban rail transit network under partial disturbances. J TRANSP ENG A-SYST 2023;149:04023114.
[26] Zhang Y, Ayyub BM, Saadat Y, Zhang D, Huang H. A double-weighted vulnerability assessment model for metrorail transit networks and its application in Shanghai metro. Int J Crit Infrastruct Prot 2020;29:100358.
[27] Zhang L, Wen H, Lu J, Lei D, Li S, Ukkusuri SV. Exploring cascading reliability of multi-modal public transit network based on complex networks. Reliab Eng Syst Saf 2022;221:108367.
[28] Lu Q, Zhang L, Xu P, Cui X, Li J. Modeling network vulnerability of urban rail transit under cascading failures: A Coupled Map Lattices approach. Reliab Eng Syst Saf 2022;221:108320.
[29] Zhang J, Min Q, Zhou Y, Cheng L. Vulnerability assessments of urban rail transit networks based on extended coupled map lattices with evacuation capability. Reliab Eng Syst Saf 2024;243:109826.
[30] Ma L, Christou V, Bocchini P. Framework for probabilistic simulation of power transmission network performance under hurricanes. Reliab Eng Syst Saf 2022;217:108072.
[31] Bellè A, Abdin AF, Fang Y, Zeng Z, Barros A. A resilience-based framework for the optimal coupling of interdependent critical infrastructures. Reliab Eng Syst Saf 2023;237:109364.
[32] Wang Y, Zhao O, Zhang L. Modeling urban rail transit system resilience under natural disasters: A two-layer network framework based on link flow. Reliab Eng Syst Saf 2024;241:109619.
[33] Almoghathawi Y, Selim S, Barker K. Community structure recovery optimization for partial disruption, functionality, and restoration in interdependent networks. Reliab Eng Syst Saf 2023;229:108853.
[34] Dehghani N L, Shafieezadeh A. Multi-stage resilience management of smart power distribution systems: A stochastic robust optimization model[J]. IEEE Trans Smart Grid 2022;13: 3452-3467.
[35] Liu W, Song Z, Ouyang M, Li J. Recovery-based seismic resilience enhancement strategies of water distribution networks. Reliab Eng Syst Saf 2020;203:107088.
[36] Xing J, Yin X, Zhang J, Chen J. Resilience modeling and improvement of metro systems considering statistical behaviors of passenger mobility. Int J Disaster Risk Reduct 2023;96:103975.
[37] Yu J, Sharma N, Gardoni P. Functional connectivity analysis for modeling flow in infrastructure. Reliab Eng Syst Saf 2024;247:110042.
[38] Wang N, Wu M, Yuen KF. A novel method to assess urban multimodal transportation system resilience considering passenger demand and infrastructure supply. Reliab Eng Syst Saf 2023;238:109478.
[39] Ma Z, Yang X, Shang W, Wu J, Sun H. Resilience analysis of an urban rail transit for the passenger travel service. Transp Res Part D 2024;128:104085.
[40] Cai B, Zhang Y, Wang H, Liu Y, Ji R, Gao C, et al. Resilience evaluation methodology of engineering systems with dynamic-Bayesian-network-based degradation and maintenance. Reliab Eng Syst Saf 2021;209:107464.
[41] He R, Tiong RLK, Yuan Y, Zhang L. Enhancing resilience of urban underground space under floods: Current status and future directions. Tunnelling Underground Space Technol 2024;147:105674.
[42] Yu X, Chen Z, Liu F, Zhu H. How urban metro networks grow: From a complex network perspective. Tunnelling Underground Space Technol 2023;131:104841.
[43] Cai B, Xie M, Liu Y, Liu Y, Feng Q. Availability-based engineering resilience metric and its corresponding evaluation methodology. Reliab Eng Syst Saf 2018;172:216–24.
[44] Wang N, Yuen KF. Resilience assessment of waterway transportation systems: Combining system

performance and recovery cost. Reliab Eng Syst Saf 2022;226:108673.
[45] Li J, Lu Q, Xu P, Liu L, Wang S. Critical station identification for cascading failure mitigation considering the Lyapunov-stability of metro stations. Reliab Eng Syst Saf 2025;256:110772.
[46] Dong X, Cui H, Su Y, Zhu M, Yao S. Identifying critical road segments and optimizing resilience strategies based on multi-state congested characteristics. Reliab Eng Syst Saf 2025;258:110912.
[47] Feng Q, Liu M, Dui H, Cai B, Fan D, Ren Y, et al. A general design-oriented resilience measurement and evaluation method for engineering systems: Resilience cube. Reliab Eng Syst Saf 2024;245:110038.
[48] Dui H, Wu X, Wu S, Xie M. Importance measure-based maintenance strategy optimization: Fundamentals, applications and future directions in AI and IoT. Front Eng Manag 2024;11:542-567.
[49] Moradi-Sarvestani S, Dehbozorgi MR, Rastegar M. A three-stage reliability-centered framework for critical feeder identification, failure modes prioritization, and optimal maintenance strategy assignment in power distribution system. Electr Pow Syst Res 2024;230:110215.
[50] Xing L, Levitin G. Connectivity modeling and optimization of linear consecutively connected systems with repairable connecting elements. European Journal of Operational Research 2018;264:732–41.
[51] Song X, Zhao P, Yin R, Zu Y, Zhang Y. Cascading failure model and resilience-based sequential recovery strategy for complex networks. Reliab Eng Syst Saf 2025;253:110488.
[52] Hu J, Wen W, Zhai C, Pei S. Surrogate-based decision-making for post-earthquake recovery scheduling and resilience assessment of subway systems considering the effect of infrastructure interdependency. Reliab Eng Syst Saf 2025;256:110781.
[53] Wang F, Tian J, Ling J, Chen Z, Xu Z. A multi-stage resilience analysis framework of critical infrastructure systems based on component importance measures. Reliab Eng Syst Saf 2025;256:110720.
[54] Zhang C, Chen R, Wang S, Dui H, Zhang Y. Resilience efficiency importance measure for the selection of a component maintenance strategy to improve system performance recovery. Reliab Eng Syst Saf 2022;217:108070
[55] Liu Z, Chen H, Liu E, Hu W. Exploring the resilience assessment framework of urban road network for sustainable cities. Physica A 2022;586:126465.
[56] Poulin C, Kane MB. Infrastructure resilience curves: Performance measures and summary metrics. Reliab Eng Syst Saf 2021;216:107926.